2014

ESTIMATING PASSIVE MATERIAL PROPERTIES AND FIBER ORIENTATION IN A MYOCARDIAL INFARCTION THROUGH AN OPTIMIZATION SCHEME USING MRI AND FE SIMULATION

Dimitri Mojsejenko
University of Kentucky, sargeantmobuto@gmail.com

STUDENT AGREEMENT:

I represent that my thesis or dissertation and abstract are my original work. Proper attribution has been given to all outside sources. I understand that I am solely responsible for obtaining any needed copyright permissions. I have obtained needed written permission statement(s) from the owner(s) of each third-party copyrighted matter to be included in my work, allowing electronic distribution (if such use is not permitted by the fair use doctrine) which will be submitted to UKnowledge as Additional File.

I hereby grant to The University of Kentucky and its agents the irrevocable, non-exclusive, and royalty-free license to archive and make accessible my work in whole or in part in all forms of media, now or hereafter known. I agree that the document mentioned above may be made available immediately for worldwide access unless an embargo applies.

I retain all other ownership rights to the copyright of my work. I also retain the right to use in future works (such as articles or books) all or part of my work. I understand that I am free to register the copyright to my work.

REVIEW, APPROVAL AND ACCEPTANCE

The document mentioned above has been reviewed and accepted by the student's advisor, on behalf of the advisory committee, and by the Director of Graduate Studies (DGS), on behalf of the program; we verify that this is the final, approved version of the student's thesis including all changes required by the advisory committee. The undersigned agree to abide by the statements above.

Dimitri Mojsejenko, Student

Dr. Jonathan F. Wenk, Major Professor

Dr. James M. McDonough, Director of Graduate Studies

ESTIMATING PASSIVE MATERIAL PROPERTIES AND FIBER ORIENTATION IN A MYOCARDIAL INFARCTION THROUGH AN OPTIMIZATION SCHEME USING MRI AND FE SIMULATION

THESIS

A thesis submitted in partial fulfillment of the requirements for the degree of Master of Science in Mechanical Engineering in the College of Engineering at the University of Kentucky

By

Dimitri Mojsejenko

Lexington, Kentucky

Director: Dr. Jonathan F. Wenk

Lexington, Kentucky

2014

ABSTRACT OF THESIS

ESTIMATING PASSIVE MATERIAL PROPERTIES AND FIBER ORIENTATION IN A MYOCARDIAL INFARCTION THROUGH AN OPTIMIZATION SCHEME USING MRI AND FE SIMULATION

Myocardial infarctions induce a maladaptive ventricular remodeling process that independently contributes to heart failure. In order to develop effective treatments, it is necessary to understand the way and extent to which the heart undergoes remodeling over the course of healing. There have been few studies to produce any data on the in-vivo material properties of infarcts, and much less on the properties over the time course of healing. In this paper, the in-vivo passive material properties of an infarcted porcine model were estimated through a combined use of magnetic resonance imaging, catheterization, finite element modeling, and a genetic algorithm optimization scheme. The collagen fiber orientation at the epicardial and endocardial surfaces of the infarct were included in the optimization. Data from porcine hearts (N=6) were taken at various time points after infarction, specifically 1 week, 4 weeks, and 8 weeks post-MI. The optimized results shared similarities with previous studies. In particular, the infarcted region was shown to dramatically increase in stiffness at 1 week post-MI. There was also evidence of a subsequent softening of the infarcted region at later time points post infarction. Fiber orientation results varied greatly but showed a shift toward a more circumferential orientation.

KEYWORDS: Myocardial Infarction, Finite Element Modeling, Ventricular Remodeling, MRI, Optimization

Dimitri Mojsejenko

4.28.2014

ESTIMATING PASSIVE MATERIAL PROPERTIES AND FIBER ORIENTATION IN A MYOCARDIAL INFARCTION THROUGH AN OPTIMIZATION SCHEME USING MRI AND FE SIMULATION

By
Dimitri Mojsejenko

_____Dr. Jonathan F. Wenk_____
Director of Thesis

_____Dr. James M. McDonough_____
Director of Graduate Studies

_____4.28.2014_____

Contents

List of Tables

List of Figures

1. Intro

An estimated 7.6 million Americans reported to have experienced a myocardial infarction (MI), a heart attack, as of the 2013 AHA Statistical Update. As disparaging as this number is, there has been great progress made in the field of cardiovascular medical therapy. From 1999-2001 to 2007-2009, there was a decrease of 34.6% in the death rate due to CHD (coronary heart disease) which includes heart attacks, angina pectoris, and stroke. Also an estimated 47% of the decrease in US deaths attributable to CHD from 1980 to 2000 was purported to be due to the increased use of evidence-based medical therapies.[1] Crucial to the development of these treatments is the understanding of the adverse ventricular remodeling process triggered by an MI. It is now a common perception that remodeling of the left ventricle independently contributes to the progression of heart failure.[2,3]

The physiological process of remodeling is defined as a change in internal structure achieved through either the reorganization of present constituents or the creation of new constituents with a different organization.[4] Thus the process inevitably changes the material properties of the structure in response to an environmental stimulus. It is a form of adaptation in which the heart seeks to return to better pump function. However, the compensatory mechanisms that promote a return to normal pump function in the short term can continue to the extent of worsening pump function and furthering maladaptive remodeling.[2] In the emerging field of mechanobiology, it is accepted that physical forces acting on cells contribute to changes in structure and function. A great example of this concept can be seen in Wolff's Law of bone transformation, from which came the accepted notion that the trabecular structure in bone results from the remodeling process governed by mechanical loads. To be more precise, the trabecular structure of bone coincides with the principal stress orientation from externally induced loads.[5] This behavior has also been seen in the healing of soft biological tissues as well, as it has been well documented that scar tissue fibers in healing wounds orient themselves in directions of tension.[6,7]

1.1 Acute Ischemia

Based on observation, the healing process of infarcted tissue is divided into four phases: acute ischemia (first few hours), necrotic (5-7 days), fibrotic (up to 2-4 weeks), and remodeling (remaining healing).[8] Acute ischemia is the phase that occurs immediately after the occlusion of a coronary artery to the onset of infarct stiffening, typically at 4-6 hours.[8] The lack of oxygen induces myocyte death in the infarcted region within the first few minutes, during which the myocardium gradually loses its active force generation in systole. The infarcted myocardium then takes on the behavior of a passive elastic material for the entire cardiac cycle. The infarct still passively stretches in the filling state of diastole, but also passively recoils during the contractive state of systole. It has been observed that the left ventricle becomes more compliant within this phase of acute ischemia. Within 30 seconds after coronary occlusion, the systolic contraction of infarcted myocardium is supplanted by passive stretching, which steadily increases over the initial 5 minutes.[8] A proposed mechanism of this increased compliance is the progressive degradation of the extracellular matrix of myocardial tissue induced by collagenolytic enzymes activated within failing myocardium.[2,3] This subsequently fosters the slippage of bundles of myocardial fibers along the cleavage planes which separate transmurally layered sheets of fibers.[2,9,10] This fiber rearrangement results in a decreased number of fibers across the wall and accounts for most of the expansion and transmural thinning of infarcted regions.[9] Furthermore, all of the thinning of noninfarcted regions is attributed to this fiber slippage along cleavage planes.[9] In a study by Weisman et al. on the mechanism of infarct expansion, it was observed that the number of myocyte bundles across the heart wall decreased in infarcted hearts exhibiting a thinning of the walls.[9] It was also found that the angles of cleavage planes relative to the endocardial surface transform to more acute angles in regions of wall thinning, supporting the proposed thinning mechanism of slippage.[9] A helpful visualization of the fiber slippage can be seen in Figure 2, in which the blackened sheet of fibers shifts between meridional and radial directions along cleavage planes.

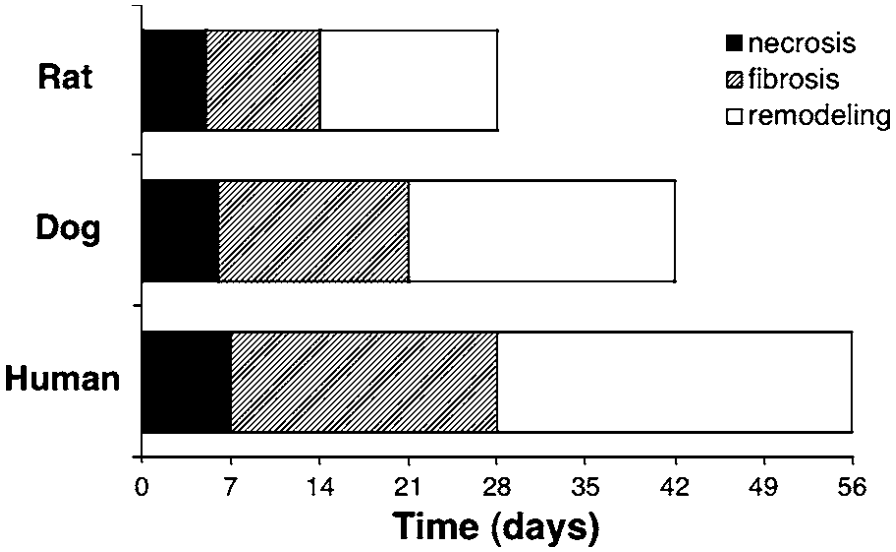

Figure 1: Time courses of healing for various animals. Image taken from Holmes, J.W.[8]

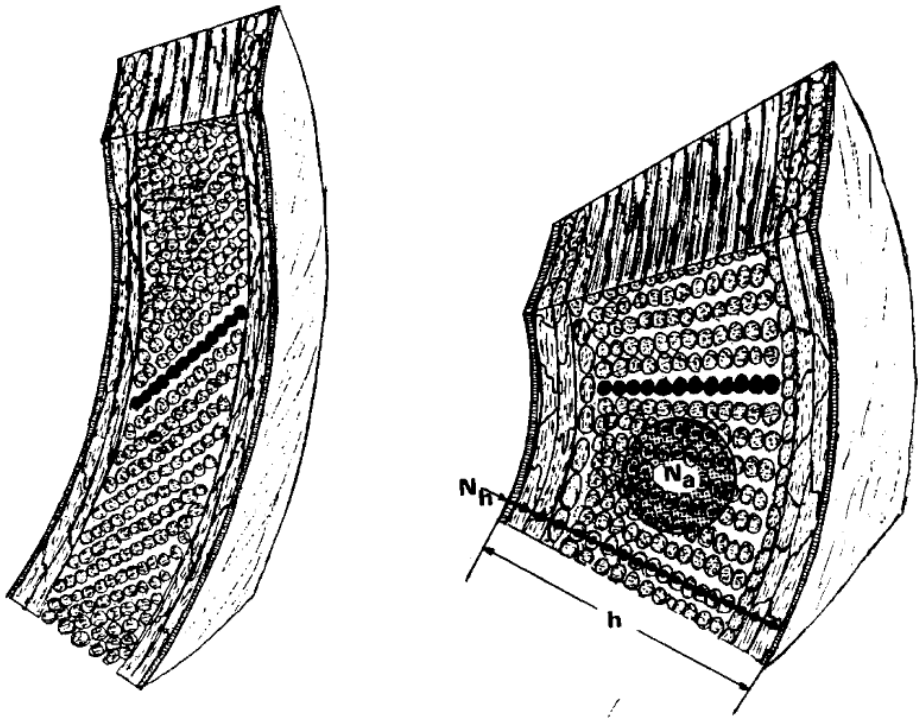

Figure 2: Schematic of myocardial fibers and cleavage planes in thin and thick myocardial walls. The mechanism believed to be responsible for the redistribution of fibers is represented by the blackened fibers. From Spotnitz, H.M.[10]

This increased compliance of the infarct causes the region to stretch and bulge at times in the cardiac cycle. In turn, energy that could normally be used to do work on blood is wasted through stretching the infarct. Furthermore ventricular dyssynchrony may develop in which differences in the timing of contractions can reduce cardiac efficiency. Stretching of the infarcted region along with global thinning of the myocardium induce a dilation of the left ventricle, and thus an increase in LV end-diastolic volume.[2,11] A consistent observation regarding left ventricle dilation is that the geometry of the remodeled heart not only expands but takes on a more spherical shape.[2] As a result of assuming a more spherical shape, displaced papillary muscles pull on the chordae tendineae connecting them to the leaflets of the mitral valve, tethering them to the extent of impeding complete valve closure.[2,12] Thus mitral valve regurgitation develops, in which there is an amount of blood that flows back into the ventricle during systolic ejection. Obviously this indicates a reduction in fraction of blood ejected and accordingly a loss in pump function.

Another mechanism contributing to a decrease in pump function is the physical coupling between the infarcted region and surrounding myocardium. Active myocytes tethered to tissue at the border of the infarct stretch the infarcted tissue in directions coinciding with the normal myocardial fiber orientation.[8] Consequently a border zone develops around the circumference of the infarct. In this border zone, the deformation and stress experienced by the noninfarcted myocardium within is regulated by the coupling with infarcted tissue.[8,13]

In an experimental study on transmural myocardial deformation, Villareal et al. found that the magnitude of normal systolic strains increased significantly from epicardium to endocardium.[14] This finding was corroborated by Xu et al. in a study involving the reconstruction of cardiac motion through tagged MRI images, in which it was found that the endocardium displayed greater motion than the epicardial wall.[15] During the ejection phase of systole, the heart is known to exhibit a twisting motion which contributes to normal pump function. This was observed in the study by Xu et al., and it is reasonable to conjecture that the gradient of motion through the heart wall has an influence on this twist. In regards to an infarcted heart, since the systolic strain was found to be uniform, the normal twisting motion may be impaired or nonexistent.

1.2 Necrosis

Following the initial phase of acute ischemia is necrosis. As mentioned previously, this phase begins at the onset of infarct stiffening and lasts about 7 days in humans.[8] In this phase there is a progression of myocardial damage from endocardium to epicardium in a sort of wavefront of injury.[16] In a study on the progression of healing of canine infarcts by Ursell et al., it was observed that ischemic injury eventually stops its advancement toward the epicardium, and muscle cells in the outer layer of epicardium actually survive.[16] It has been suggested that this functioning layer of epicardial tissue plays an integral role in formation of the border zone.[16] One of the mechanical changes observed in a necrotic infarct is an increase in circumferential and longitudinal stiffness under multiaxial loading.[8] However there is no apparent change in stiffness in uniaxial tests, which implies an advance in the mechanical coupling between circumferential and longitudinal directions, possibly due to collagen cross-linking.[8] Another mechanical change of the infarcted region is the increase in unstressed segment length of fibers below end-diastolic pressure and a decrease in segment lengths at higher pressures.

The most likely explanation for the increase in infarct stiffness is the presence of interstitial edema, which has been thoroughly documented to occur in ischemic hearts.[16] A substantial piece of evidence for this comes from an experimental study by Amirhamzeh et al., in which edema induced in the hearts of pigs was shown to significantly increase LV stiffness.[17] The decrease in infarct compliance is counterbalanced by the response of anti-inflammatory agents promoting expansion by reducing edema. In regards to the increase in unstressed segment length, the most likely explanation is infarct expansion as described in the section on acute ischemia. Although signs of necrosis may persist for weeks to months in large animals, the necrotic phase ends once the infarct starts to experience a rapid increase in the number of fibroblasts and amount of new collagen.[8]

1.3 Fibrosis

In the fibrotic phase of healing, the deposition of new collagen is the main source of change in structure and mechanical properties. The amount of collagen present in healing myocardium is known to increase from 1 to 6 weeks after infarction in dogs,

sheep, and rats, as well as humans.[8,18] Besides the increase in collagen, there is also a change in the type of collagen deposited. As part of a study by Rich and Whittaker, the collagen content in the scarred myocardium of rats was found to increase from 61% to 83% to 95% at 1,3, and 5 weeks after injury respectively.[19] Comparing data at 5 weeks to that at 1 week, the percentage of thin fibers decreased from 43% to 4% whereas the percentage of thick fibers increased from 13% to 65%.[19] The thin fibers have been suggested to be type III collagen while the thick fibers represent type I collagen, and it has been proposed that the early appearance of the type III collagen provides a scaffold for the fabrication of the thicker type I collagen.[13] It has been consistently observed that type I collagen predominantly orients itself in the circumferential direction in healing myocardial scar tissue.[8,13,20] This agrees well with a study by Holmes et al. in which the average collagen fiber direction across the majority of the heart wall was observed to align within 30^0 of the circumferential direction in 3 week old porcine infarcts.[20] Also, infarct shrinkage was found to occur predominantly in the circumferential direction at 3 weeks into healing for porcine hearts.[20] Some of the best data available on the anisotropy of infarcts comes from a study by Gupta et al., in which the progression of stiffness in porcine anteroapical infarcts was observed.[21] The results of which can be seen in Figure 3, where circumferential and longitudinal stresses are presented for the various phases of healing. Notice how the overall stiffness of the infarct initially increases from the acute ischemic phase to the fibrotic phase and then decreases through the remodeling phase. Also evident from the plot is the switch in anisotropy that occurs during the fibrotic phase, in which the infarct transforms from a more longitudinally stiff region to one more circumferentially stiff, consistent with the orientation of collagen deposition mentioned previously.

Due to increased infarct stiffness, the left ventricle may not be allowed to expand fully resulting in an impairment of diastolic filling, which severely limits pump function.[8] The aforementioned coupling between the stiff infarct and adjacent non-infarcted myocardium limits the diastolic stretch of functioning myocardium, thereby reducing systolic contraction and thus pump function.[8] The fibrotic phase of healing is said to end when collagen accumulation slows and mechanical properties decouple from collagen

content.[8] According to the results of Holmes et al. this occurs at approximately 4 weeks in humans and around 3 weeks for other large animals, as can be seen in Figure 1.

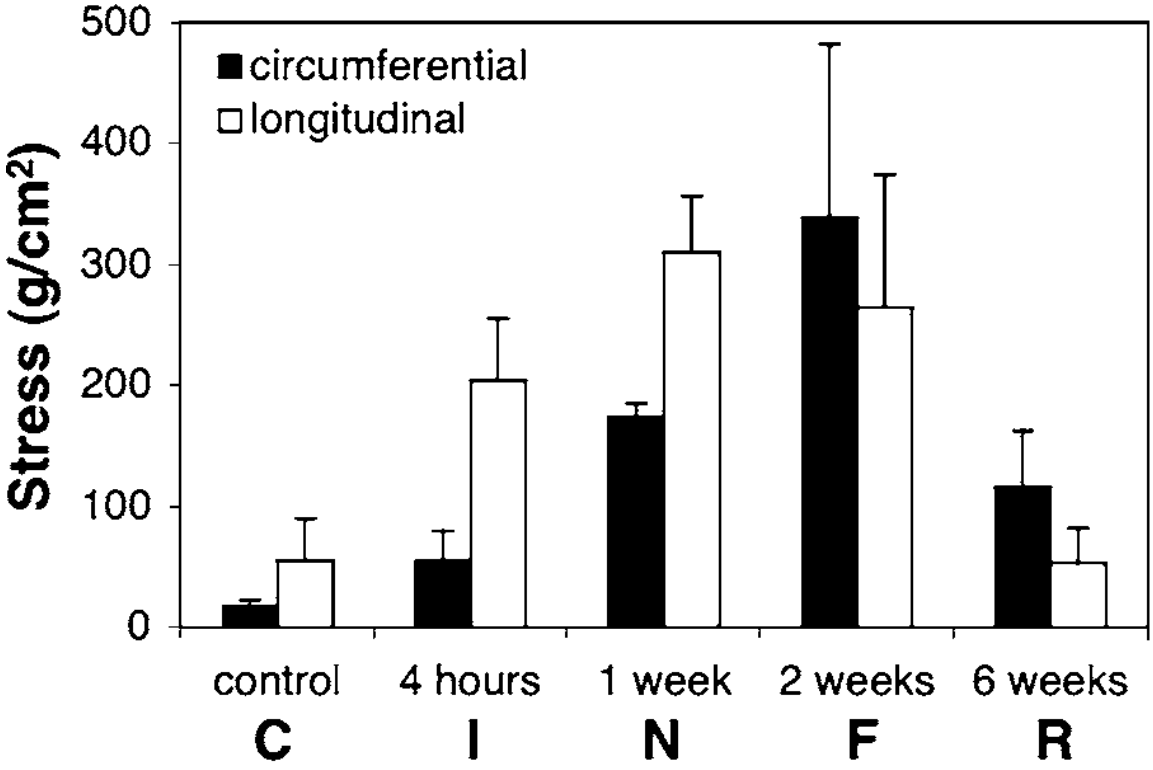

Figure 3: Development of anisotropy in healing ovine infarcts. The graph displays circumferential and longitudinal stresses during 15% equibiaxial extension of excised infarcts. The labels along the bottom represent the phases of healing: control (C), acutely ischemic (I), necrotic (N), fibrotic (F), and remodeling (R). Data comes from Gupta, K.B.[21] Graph comes from Holmes, J.W.[8]

1.4 Remodeling

Although collagen content may continue to rise for several weeks, there is a decrease in infarct stiffness in the remodeling phase, as can be seen in Figure 3.[21] This suggests that there must be other factors other than collagen content governing the mechanics. One such factor that seems to correlate with observed mechanics of the remodeling phase is the cross-linking of collagen, which continues to increase despite a plateau in the rate of collagen production. Also evident from Figure 3, the longitudinal stiffness is shown to equalize at about the same level as that of the non-infarcted control myocardium, whereas the circumferential stiffness remains elevated above control and nearly twice that of the longitudinal. The similar longitudinal stiffness for the infarct and adjacent non-infarcted myocardium serves to minimize the negative effects of the

mechanical tethering at the border zone. Although the circumferential stiffness remains elevated, its decline is characteristic of a move toward normal diastolic function while compensating for the increased stresses experienced by the infarct. Throughout the remodeling phase, the heart is continuously shaped by all of the compensatory mechanisms prevalent in the previous phases. This process of adaptation may continue indefinitely in pursuit of a stable configuration.

1.5 Modeling myocardial mechanics

The methods of determining material properties of myocardium by in vitro means has been the standard approach for many years. Although in vitro data has provided much insight on myocardial mechanics and still is completely necessary for other approaches, alone it does not allow for an accurate view of the dynamic physiological processes that occur in vivo. The call for an in vivo approach has eventually led to the use of an inverted finite element method. The classic solid mechanics problem is to determine the motion that is induced in a given material by an applied load. In the inverse problem, material properties are sought once given the motion and applied load.

Based on the observations of myocardium, such as those from histology or mechanical testing on excised samples, there have been many attempts to characterize the stress-strain relationship that governs its deformation. Biaxial tissue testing has remained a valuable tool for characterizing the three dimensional mechanical properties of myocardium.[22] In perhaps the first biaxial extension tests of excised myocardium, Demer and Yin (1983) reported myocardium to exhibit non-linear elasticity and viscoelasticity as well as anisotropic behavior.[23] Therefore myocardium is typically modeled under finite hyperelasticity. Also referred to as a Green elastic material, a hyperelastic material assumes the existence of a strain energy function, from which a stress-strain relationship is derived. The strain energy must vanish over a complete cycle of deformation for such a material. Upon formulating a mechanical power balance and rearranging terms, the constitutive relation for an incompressible material under isothermal finite hyperelasticity can be written as

$$\boldsymbol{S} = \frac{\partial W}{\partial \boldsymbol{E}} - pJ\boldsymbol{E}^{-1} \tag{1}$$

where **S** is the 2nd Piola-Kirchoff stress, W is the strain energy function, **E** is the Lagrangian strain, p is a Lagrange multiplier, and J is the Jacobian of the deformation gradient.

The functional form of the strain energy function W varies, dependent on the approach used to determine it. One common approach is to estimate the form of W by curve-fitting experimental measurements, as performed in the study mentioned previously by Gupta et al. (1994).[21] Similarly Humphrey et al. proposed a polynomial form of W, determined directly from experimental protocols in which one of two coordinate invariant measures of finite deformation was held constant while the other was varied.[24] The major difficulty with any constitutive model based solely on mechanical testing of excised tissue is the uncertainty as to how structural interactions between myocardial constituents influence behavior in vivo.[22] In a study by Guccione et al. (1991) passive material parameters of an intact canine left ventricle were optimized for a transversely-isotropic hyperelastic constitutive law.[25] Many have employed this constitutive model to estimate in-vivo myocardial material properties, going further by generating anatomically accurate geometry contoured from MRI data. Fortunately with advances in medical imaging, techniques have been developed that employ a combination of MRI, catheterization, and finite element modeling to estimate in-vivo mechanical properties of myocardium. Once a constitutive relation is implemented into a finite element model with given pressure loads, computationally determined strains can be compared with experimentally measured MRI strain data until an optimized set of parameters can be reached.

Augenstein et al. used SPAMM (SPAtial Modulation of Magnetization) MRI, catheterization, and 3D FE modeling to estimate the material properties of an isolated arrested pig heart that underwent passive inflation.[26] Of particular interest, muscle fiber architecture obtained from diffusion tensor imaging was included in the model, instead of using histological data. Sun et al. estimated active material properties in the non-infarcted myocardium of a sheep LV 8 weeks post-MI using 3D tagged MRI, catheterization, FE modeling, and a successive response surface method for optimization.[27] Wenk et al. used the same approach to estimate active properties of the remote, border zone, and infarct regions of a sheep LV 8 weeks after the induction of a posterobasal MI.[28]

In each of the studies on in-vivo or isolated hearts mentioned previously, the focus was on determining properties of viable myocardium. However there have been no studies that determined the in-vivo passive material properties of infarcted myocardium. In the current study, the goal was to determine in-vivo material properties of both infarcted and remote myocardium in a porcine model over the time course of a healing MI. Additionally the orientation of collagen fibers in the infarcted region were allowed to be optimized with the material properties, instead of being assigned a priori. There was a study by Nair et al. in which myocardial fiber angles of a healthy rabbit heart were found through an optimization using 3D FE modeling, epicardial surface strain data, and a genetic algorithm scheme.[29] The model was simple and only 2 points of strain were compared in the optimization. However the study showed the benefit of using genetic algorithms for estimating myocardial material parameters. In the current study, a combination of MRI, catheterization, and 3D FE modeling were used to create animal specific models of infarcted pig hearts. The material parameters were then determined through an optimization scheme that minimized the difference between in-vivo strains and volume obtained from MRI and model predicted strains and volume.

2. Methods

2.1 Animal Model

The animals used in this work received care in compliance with the protocols approved by the Institutional Animal Care and Use Committee at the University of Pennsylvania in accordance with the guidelines for humane care (National Institutes of Health Publication 85-23, revised 1996).

Myocardial infarction was induced in adult male Yorkshire swine (N=6) weighing approximately 40 kg. The pigs were anesthetized and the LV free wall exposed through a left thoracotomy. A posterior MI was induced by suture ligation of the left circumflex artery (LCX) and select obtuse marginal (OM) branches. An example of the ligature points for one of the cases is shown in Figure 4. Although the ligation sites varied slightly between animals, the procedure was performed in such a way to produce consistently sized infarcts comprising 20-25% of the left ventricle.[30] Resulting from this ligation approach, infarcts were produced with a congruity in size, shape, and location between

animals. Ten MRI compatible platinum wire markers were sutured to the epicardium around the infarct periphery immediately following infarction to enable infarct contouring from subsequent MRI acquisitions. It should be noted that thirty minutes post-MI, the pigs received twenty 0.3 mL injections of saline in the infarct, since they were also being used as controls in a biomaterial injection study.

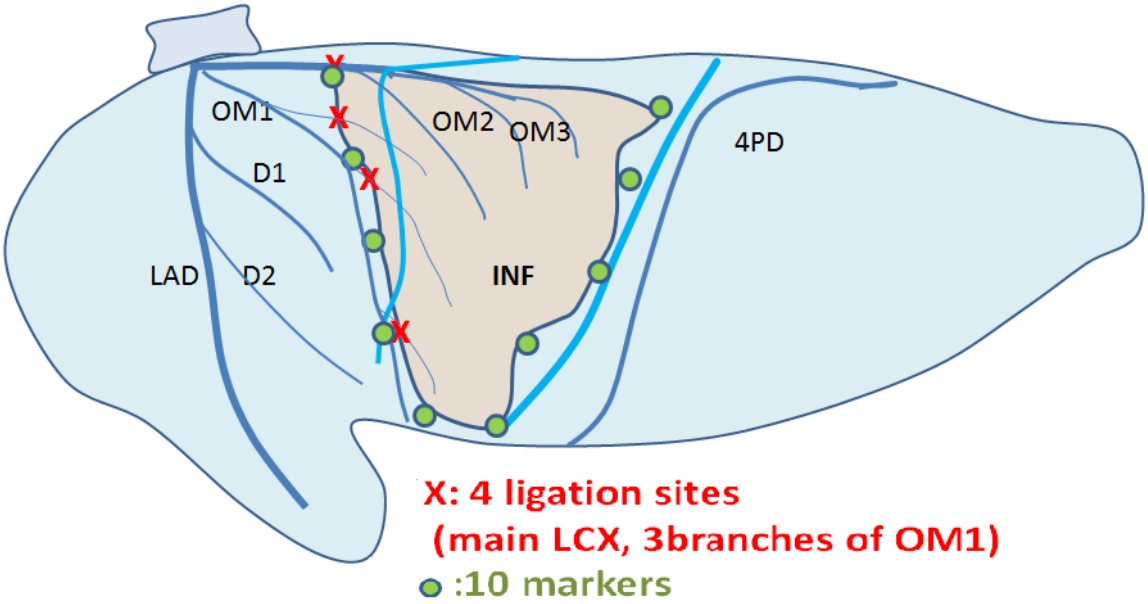

Figure 4: Coronary artery ligation pattern for case 2. A total of ten platinum markers mark the periphery of the infarcted region.

2.2 MRI Acquisition and Image Analysis

Cardiac MRI scans were performed at 1, 4, and 8 weeks post-MI using a 3T Siemens Trio A Tim Magnetom scanner (Siemens; Malvern, PA). For each MRI scan, a high fidelity pressure transducer (Millar Instruments; Houston, TX) was guided into the LV for cardiac gating. The measured pressure was later used to load the FE model. Images were collected using two techniques: 1) 3D SPAMM was performed in order to assess regional wall strain and 2) late-gadolinium enhanced (LGE) images were taken to further define the infarct area Figure 5. The endocardium and epicardium of the LV were contoured from the 3D SPAMM images using ImageJ software (NIH; Bethesda, MD). The reference contours were generated at early diastolic filling Figure 5, following

isovolumic relaxation, in order to generate the animal-specific ventricular geometry. Additionally, the endocardium was contoured at end-diastole in order to calculate LV volume. Infarct boundaries were created by identifying the platinum epicardial markers in the 3D SPAMM images. The total infarct area was confirmed by comparing marker positions with the enhanced region in the LGE images. Diastolic strain was calculated from the 3D SPAMM images using a custom optical flow plug-in for ImageJ to derive 3D displacement flow fields.[15] It should be noted that the LV strain, volume, and contour data were all generated from the 3D SPAMM images and matched with simultaneous pressure measurements, ensuring continuity between all data used to generate the model.

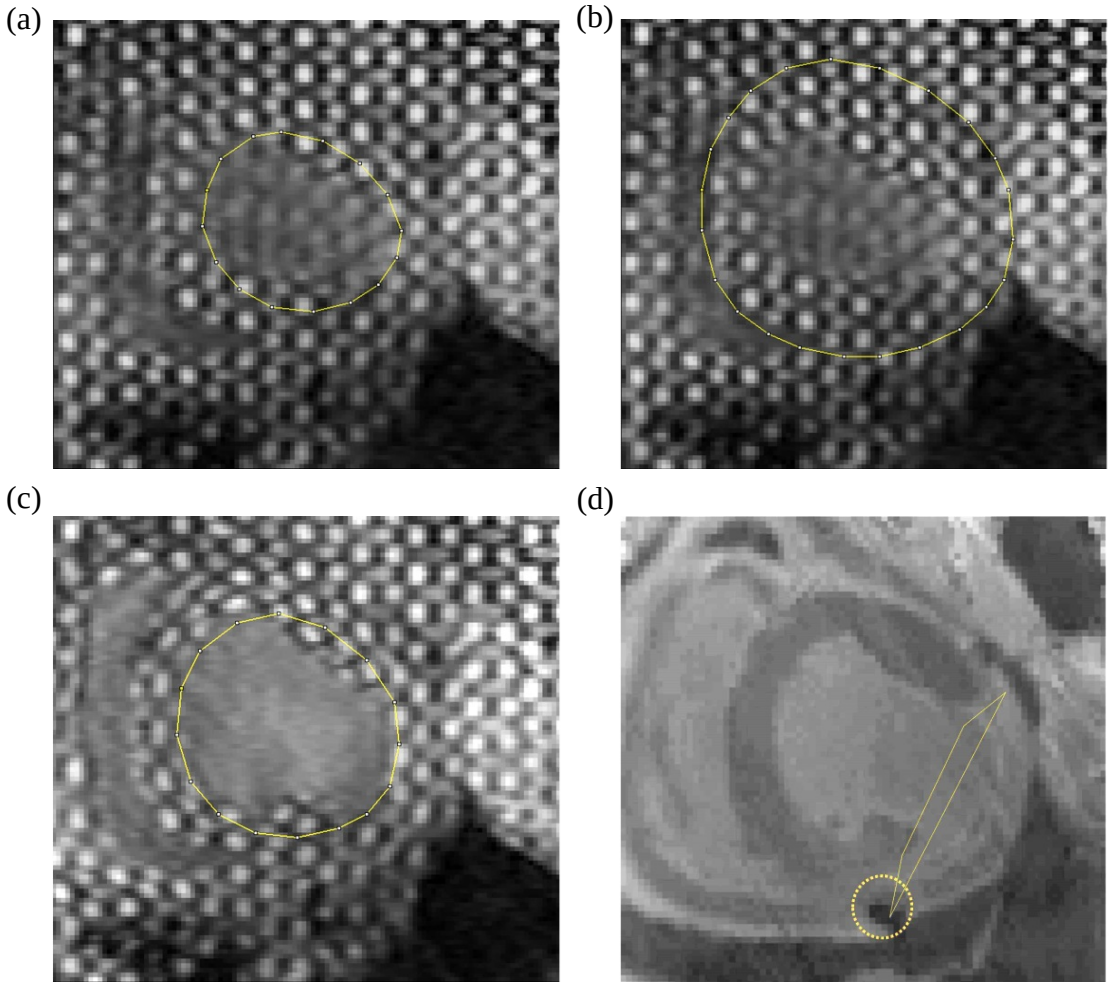

Figure 5: Short axis view of 3D SPAMM images from case 1 at early diastole with (a) endocardial and (b) epicardial contours, and short axis view at end-diastole with (c) endocardial contour. Short axis view of LGE image at (d) early diastole, with marker circled and boundaries defined.

2.3 FE Model

The reference state for the FE model was taken to be at early diastole, where LV pressure is at a minimum and is therefore closest to an in-vivo stress-free state. Each set of endocardial and epicardial reference contours were fit with 3D surfaces to represent the animal-specific geometry (Rapidform; INUS Technology, Inc., Sunnyvale, CA). The boundary between the infarct and remote region was defined using 3D spline curves that were created by visually tracing infarct marker positions from MR images and then projecting onto the endocardial and epicardial surfaces. The FE mesh was produced by filling the volume between endocardial and epicardial surfaces with hexahedral brick elements incorporating a trilinear interpolation scheme (TrueGrid; XYZ Scientific, Inc., Livermore, CA, USA). The wall of each FE model consisted of 3 elements transmurally, 36 elements circumferentially, and 12 elements longitudinally, with a patch of 192 elements at the apex. A transmural thickness of three elements deep was previously found to be sufficient for accurate volume calculations while maintaining computational efficiency.[27] The infarct and remote regions were designated as two separate materials, allowing for different properties to be assigned to each, which can be seen in Figure 6. The inner endocardial surface was lined with linearly elastic shell elements to create an enclosed airbag for computing left ventricle cavity volume. The airbag had no influence on the mechanical response of the myocardium, as it was modeled as extremely soft with a Young's modulus of 1×10^{-10} kPa and Poisson's ratio of 0.3.

Myofiber angles were assigned to each hexahedral element using a custom MATLAB script. The angles were appointed at the endocardial and epicardial surfaces and varied linearly through the transmural thickness. For the remote region at 1 and 4 weeks post-MI, angles were fixed at -37 degrees at the epicardium and 83 degrees at the endocardium, with respect to the circumferential direction, based on previous studies with porcine ventricles.[31] At 8 weeks post-MI the remote fiber angles were set at -27 degrees at the epicardium and 88 degrees at the endocardium, with respect to the circumferential. This was done in accordance with results of a study performed by Mekkaoui et al. in which a technique for quantitative 3D diffusion CMR tractography of the heart was developed. Diffusion tensor MRI data was taken for normal human, sheep, rat, and 3 month post-MI infarcted sheep. A significant positive shift in helix angle was

observed in the remote region of the infarcted sheep as shown in Figure 7, and was confirmed histologically as seen in Figure 8.

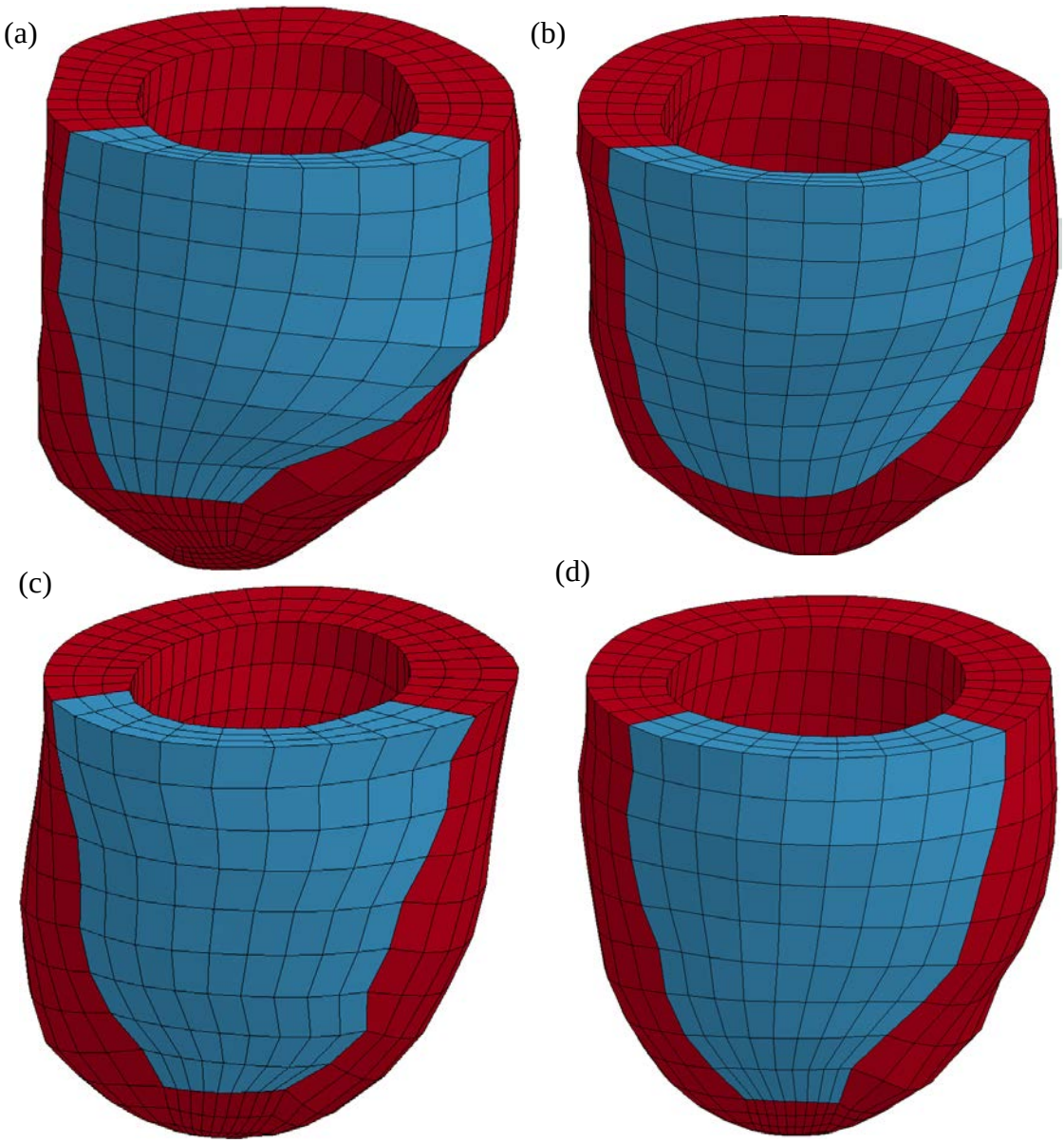

Figure 6: Finite element models of infarcted porcine LV at 4 weeks post MI for (a) case 1, (b) case 3, (c) case 4, (d) case 5, and (e) case 6. The infarcted regions are shown as blue elements and the remote as red.

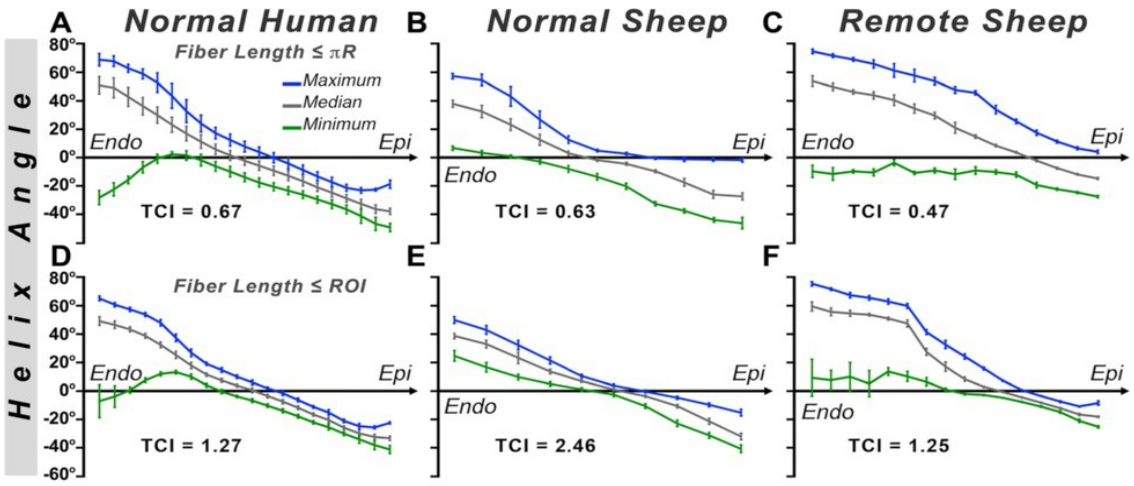

Figure 7: Helix angle curves for the lateral wall of (A-D) a normal human heart, (E-H) a normal sheep heart, and (I-L) the remote zone of a sheep heart with an anteroseptal infarct. The image comes from the study by Mekkaoui et al.[32]

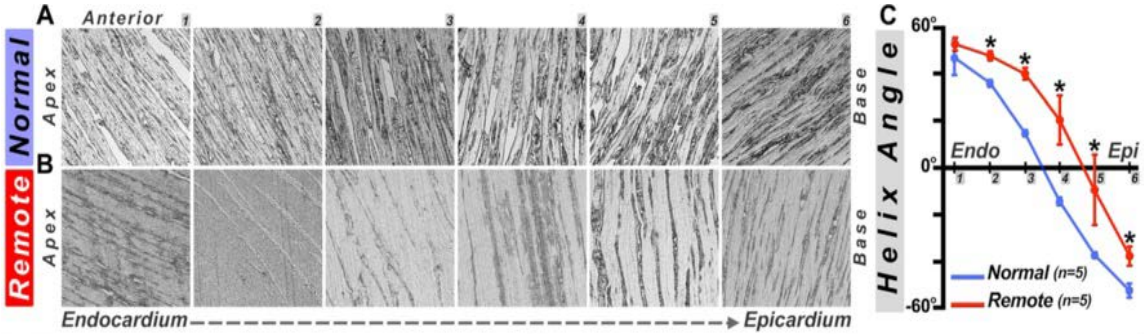

Figure 8: Comparison of histological sections taken from the lateral wall of (A) a normal sheep heart and (B) the remote zone of an infarcted sheep heart 3 months post-MI. A rightward shift of fibers in the remote zone is evident. Transmural gradient in helix angle calculated from histological sections were used to create the plot in (C). Each of these figures was taken from the study by Mekkaoui et al.[32]

The fiber angles in the infarct region were parameterized as part of the optimization, which will be discussed in a later section. Boundary conditions were implemented at the base of the LV to fully constrain displacement on the epicardial-basal edge, while allowing the remaining basal nodes to move in the circumferential-radial plane. The endocardial wall was loaded with a pressure boundary condition, which was based on the time course of the measured animal-specific diastolic pressure.

The implementation of myofiber geometry into the FE model is becoming standard in the modeling of myocardium, as it has proven to be a key impetus of ventricular mechanics and remodeling. Historically, this has been done through histological studies, although as technology progresses, noninvasive imaging techniques are seeing increased success and popularity. These imaging techniques include diffusion tensor MRI, quantitative ultrasonic backscatter, and echocardiography-based shear wave imaging.[7,31,33-35] There has been much success in determining the fiber architecture of normally functioning myocardium; however, the fiber architecture of infarcted regions remains resistant to measurement. In a 3D DT-MRI study on the fiber architecture of infarcted porcine hearts by Zhang et al., regions displaying DT-MRI fiber disruptions corresponded to infarcted areas.[33] Nonetheless, in the study by Wickline et al., the use of an ultrasonic backscatter imaging technique provided the ability to determine the transmural shift in fiber orientation per millimeter of tissue for both healthy and infarcted regions.[7] Unfortunately, this data was not useful to this study as there was no reference angle given from which to interpret the transmural shift.

2.4 Constitutive Model

The material response of the myocardium was assumed to be nearly incompressible, transversely isotropic, and hyperelastic. Since only the passive mechanics were investigated in this study, there was no need for including the active contraction of systole into the model. The diastolic mechanics are described by the strain energy function for passive myocardium developed by Guccione et al, in which a Fung-type exponential relation is used (2)

$$W = \frac{1}{2}C(e^{Q} - 1)$$

with transverse-isotropy given by

$$Q = b_f E_{11}^2 + b_t(E_{22}^2 + E_{33}^2 + E_{23}^2 + E_{32}^2) + b_{fs}(E_{12}^2 + E_{21}^2 + E_{13}^2 + E_{31}^2)\ . \quad (3)$$

The constants C, b_f, b_t, b_{fs}, are diastolic myocardial material parameters, whereas E_{11} is the Green-Lagrange strain in the fiber direction, E_{22} is the cross-fiber in-plane strain, E_{33} is the radial strain transverse to the fiber direction, and the rest are shear strains.[4,25] This strain energy function, used to describe both remote and infarct regions, was implemented through the use of a material subroutine in the FE solver LS-DYNA (Livermore Software Technology Corporation, Livermore, CA, USA).

2.5 Optimization

The optimization problem was performed with the use of the commercial FE optimization software, LS-OPT (Livermore Software Technology Corporation, Livermore, CA), which with the use of statistical and optimization methods is able to explore a design space and find an optimal design. A genetic algorithm (GA) technique was chosen for the optimization, due to the large number of parameters to be optimized, and was performed using the software LS-OPT (Livermore Software Technology Corporation, Livermore, CA). Genetic algorithms perform well as global optimizers, whereas gradient-based methods can get stuck in local optima when exploring a large parameter space.[36] In the study by Nair et al. (2007) GAs were found to be a robust method for optimizing cardiac material parameters in 3D models.[29]

A total of 10 parameters were optimized in the current study. These included the diastolic material parameters from the strain energy function (C, b_f, b_t, b_{fs}) for both the remote and infarct regions, as well as the epicardial and endocardial fiber angles in the

infarct. For the infarct, the fiber angles were assumed to vary linearly, as in the remote region. The ranges that were defined for each parameter are given in Table 1. These values were found to provide sufficient space for the optimization to converge without the bounds driving the solution. It was discovered that using shorter infarct angle ranges, instead of full 90 degree sets, provided better convergence to the global optimum. Also the range for the endocardial fiber angle was shifted toward a more circumferential alignment in accordance with observations made by Holmes et al., in which 3 week old porcine infarcts were observed to exhibit average collagen fiber directions within 30% of circumferential across the majority of the wall.[20]

Table 1: Optimization Parameter Ranges

(a)

		Min	Max
Remote	C (kPa)	0.1	10
	b_f	1	100
	b_t	1	50
	b_{fs}	1	50
Infarct	C (kPa)	0.1	25
	b_f	1	250
	b_t	1	60
	b_{fs}	1	60
	epi-angle (deg)	-50	0
	endo-angle (deg)	40	90

(b)

		Min	Max
Remote	C (kPa)	0.1	10
	b_f	1	100
	b_t	1	50
	b_{fs}	1	50
Infarct	C (kPa)	0.1	25
	b_f	1	250
	b_t	1	60
	b_{fs}	1	60
	epi-angle (deg)	-50	0
	endo-angle (deg)	0	50

Table 1: Optimization parameter ranges used in the 1week cases are given in (a) whereas the ranges for the other time points are given in (b).

The objective function that was minimized during the optimization was taken to be the mean squared error (MSE) between experimentally measured and FE predicted strains at an array of points in the midwall of the LV. Specifically, the centroids of midwall elements were compared to the nearest LV points from the MRI data where strain was measured. This was possible because the LV contours used to generate the FE model and experimental strain points were from the same 3D SPAMM data. A total of seven rings of elements starting from the base, excluding the first ring, were used for the

strain comparison. This led to a total of 252 points where strain was compared. Additionally the difference in LV cavity volume was added to the objective function and carried an equal weight as that of the strain points. The MSE was defined as

$$\mathrm{MSE} = \sum_{n=1}^{N} \sum_{\substack{i=1,2,3;\\ j=1,2,3;}} w_n \left(E_{ij,n} - \overline{E}_{ij,n} \right)^2 + \sum_{m=1}^{M} w_m \left(\frac{V_m - \overline{V}_m}{\overline{V}_m} \right)^2 \tag{4}$$

where n is the strain point, N is the total number of strain points, $E_{ij,n}$ is the computed FE end-diastolic strain at each point, and V_m is the computed FE end-diastolic LV volume. The overbar represents animal-specific *in-vivo* measurements. An additional constraint was placed on the volume to ensure that it stayed bounded within ±5% of the experimentally measured volume.

A flowchart of the optimization process can be found in Figure 9. Briefly, the process begins with the generation of an initial population of 100 random designs. A "design" is a unique combination of the 10 parameters within each respective range, which are assigned to the FE model. After some initial testing, it was found that the population size of 100 FE simulations over 30 generations (iterations) allowed the genetic algorithm to produce consistently optimized results. After the initialization, a custom MATLAB script takes the fiber angles and modifies the fiber architecture of the FE model for each of the 100 designs. LS-DYNA then runs the FE simulations for each model, after which LS-OPT begins the optimization process.[36] The designs are analyzed using the objective function defined previously. The 2 designs with the lowest MSE are saved for the next generation in a process called elitism. A tournament selection was chosen as the reproduction operator; in accordance, two individual designs are randomly selected and the one with the lowest MSE is chosen to participate in mating. The designs of the next generation, the children, are created through an exploration operator referred to as crossover. This operator randomly selects a number of parents to mate to produce a number of children. The children carry qualities of each of their parents in the sense that their parameter values are the same as that of a parent or somewhere between the ranges of the parents. Using the standard (2,2) strategy for crossover, two children are created by and replace two parents. Therefore the sole victor decided in the tournament selection mates with each of the other 99 designs in the generation. Mutation is also involved in the

creation of the child population and incites random changes in parameters based on a designated mutation probability. Once the child population of 100 is created, the 2 with the highest MSE are replaced by the 2 elites saved from the parent population. Hence the new generation is fully created and the process continues with the creation of the next set of models and simulations.

2.6 Simulated Equi-biaxial Extension

In order to facilitate a clearer interpretation of the material parameters, equi-biaxial extension tests were simulated using the parameters determined from the optimization. The constitutive law, given in Eqn. (2) and (3), was formulated for the case of planar equi-biaxial extension, as shown by Guccione et al.[25] The resulting stress-strain equations were implemented into an in-house MATLAB script, where stress was calculated at the same set of strain points for each case. In the formulation, the fiber and cross-fiber directions were assumed to align with the loading directions. Additionally, the simulated sample was assumed to be a thin, incompressible segment of tissue in which there were no changes in fiber orientation through the thickness.

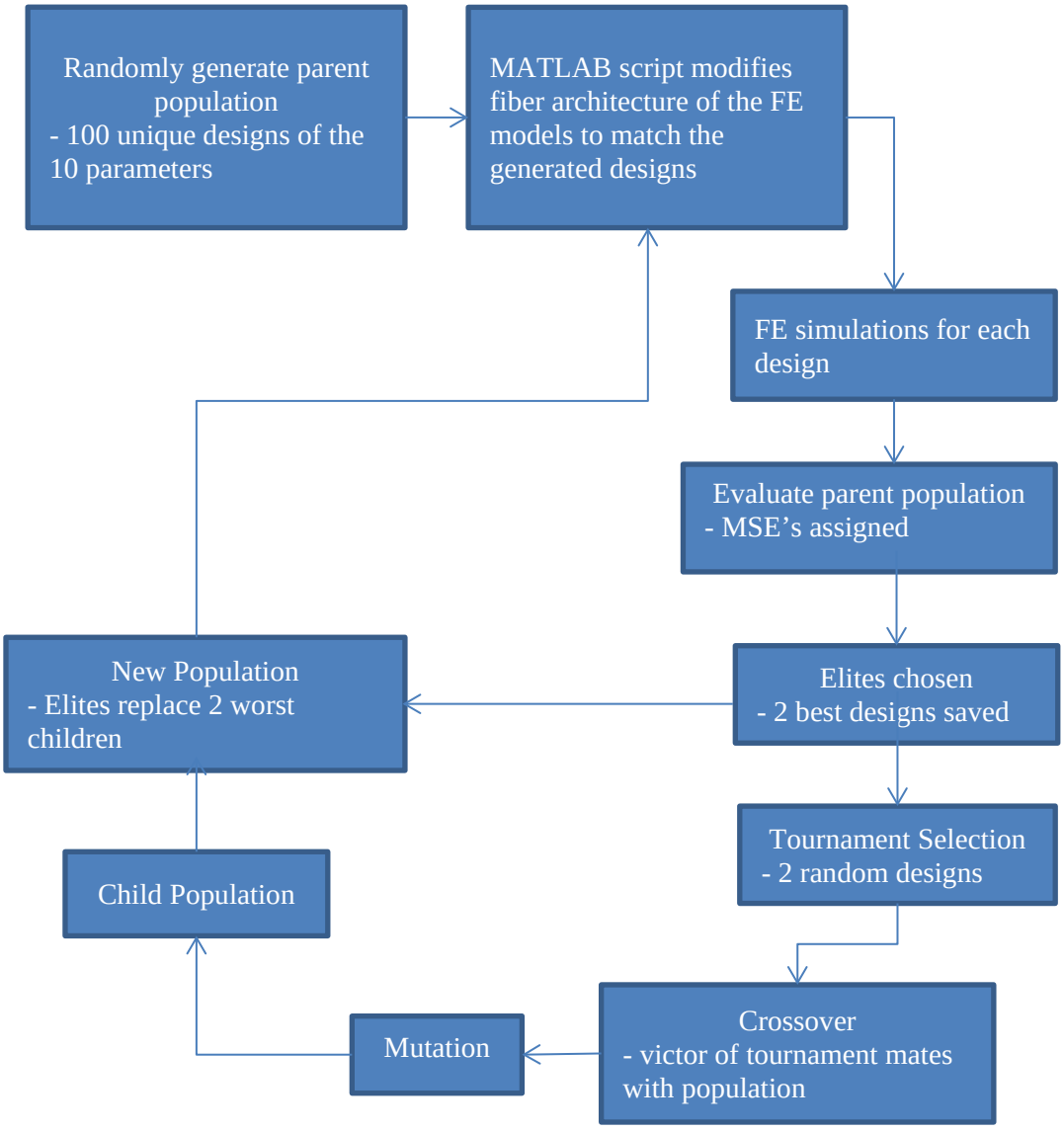

Figure 9: Flowchart of the optimization procedure showing the loop for a single generation.

3. Results

The optimizations were each allowed to run for 30 generations, and it was found that this allowed sufficient time for convergence to an optimal set of material parameters. The optimization software LS-OPT offered a rather functional visual interface with which to view the results of optimization runs. A couple examples of visualizations created through LS-OPT can be seen in Figure 10, which specifically shows the optimizations results for case 4 at 1 week post-MI. In Figure 10 (a) the design points for all of the generations can be seen filling the parameter space. The 3D plot presents full ranges of two infarct material parameters, so one may view how thoroughly the GA searched the parameter space over the course of the optimization. Also provided by the figure is a color bar indicating the generation in which each design point was created. Notice the even distribution of design points from early generations and how they can vary greatly in MSE, the vertical axis. Design points tend to congregate in ever compacting clouds of increasingly low MSE values in the latest generations. The convergent cloud of design points can be seen more clearly in Figure 10 (b), showing the convergence of material parameter $b_{f,infarct}$. Here the colors indicating the generations are easier to identify, and one can see how designs from later generations generally produce lower MSE values as the optimization hones in on the optimum.

The span of all design points for all generations of case 3 at 8 weeks post-MI can be seen in Figure 11. The feasibility of each design is also given, where designs which violate the volume constraint are designated infeasible. Notice the dense clustering around lower values of the parameter C for the remote region. In fact, past the 5^{th} generation there aren't any more feasible designs with a value for C higher than 2. The parameter C for the remote region quickly levels off near 1, whereas C for the infarct gradually becomes bounded between values of 10 and 20.

Figure 12 shows how material parameter values change over the course of the optimization. The plots in Figure 12 are from data of the best results, lowest MSE, of each generation for case 2 at 1 week post-MI. The values of the non-angle parameters were normalized by their respective parameter ranges given in Table 1. Notice how rapidly the parameters vary in the early generations as the optimization explores the full paramter space. The parameter C for both the remote and infarcted regions is one of the

first to level off and stays nearly constant after the 10^{th} generation. All of the parameters appear to be optimized by the 24^{th} generation, which is where the optimal paramter set was found for case 2 at 1 week post-MI.

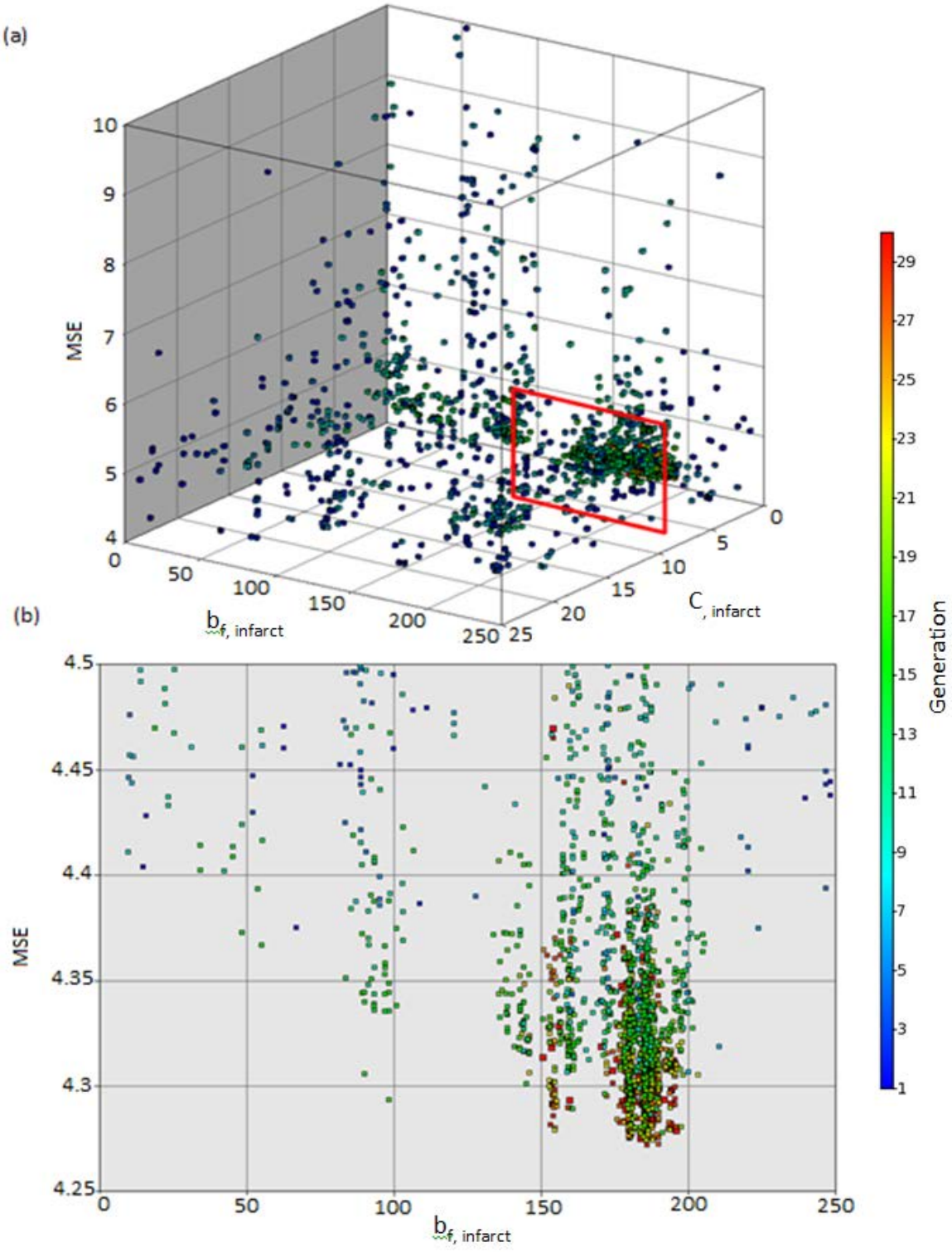

Figure 10: Optimization results for case 4 at 1 week post-MI depicting two infarct parameters. (a) 3D plot of $\mathbf{b_f}$ versus C with the MSE on the vertical axis. Each point represents a unique design generated by the optimization. (b) 2D slice of plot (a) with $\mathbf{b_f}$ versus MSE. The converging cluster of points coincides with the red boxed area in (a).

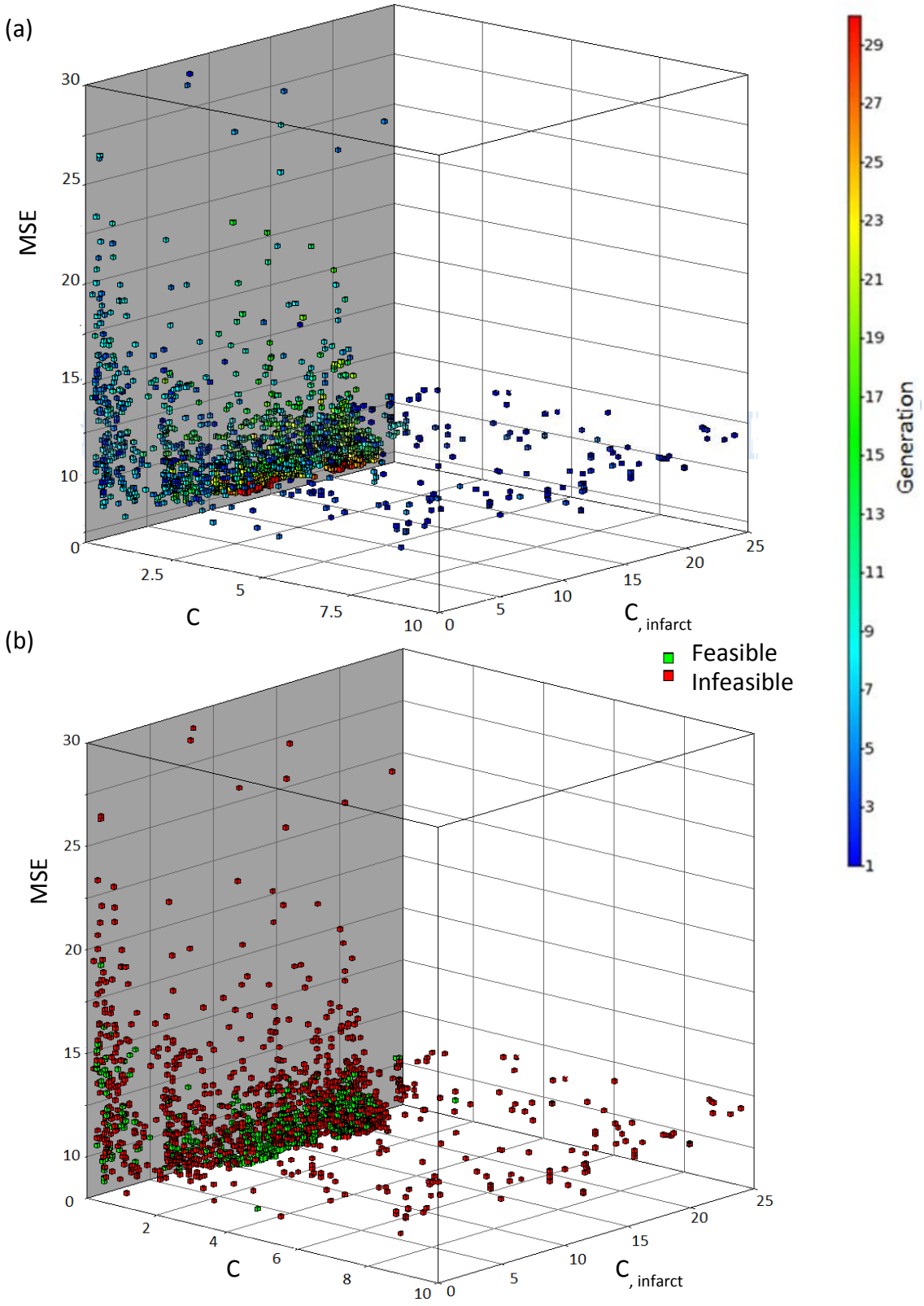

Figure 11: Optimization results for case 3 at 8 weeks post-MI depicting the parameter C for both the remote and infarct regions. The 3D plot in (a) gives all of the designs from every generation, whereas the feasibility of each design point is shown in (b).

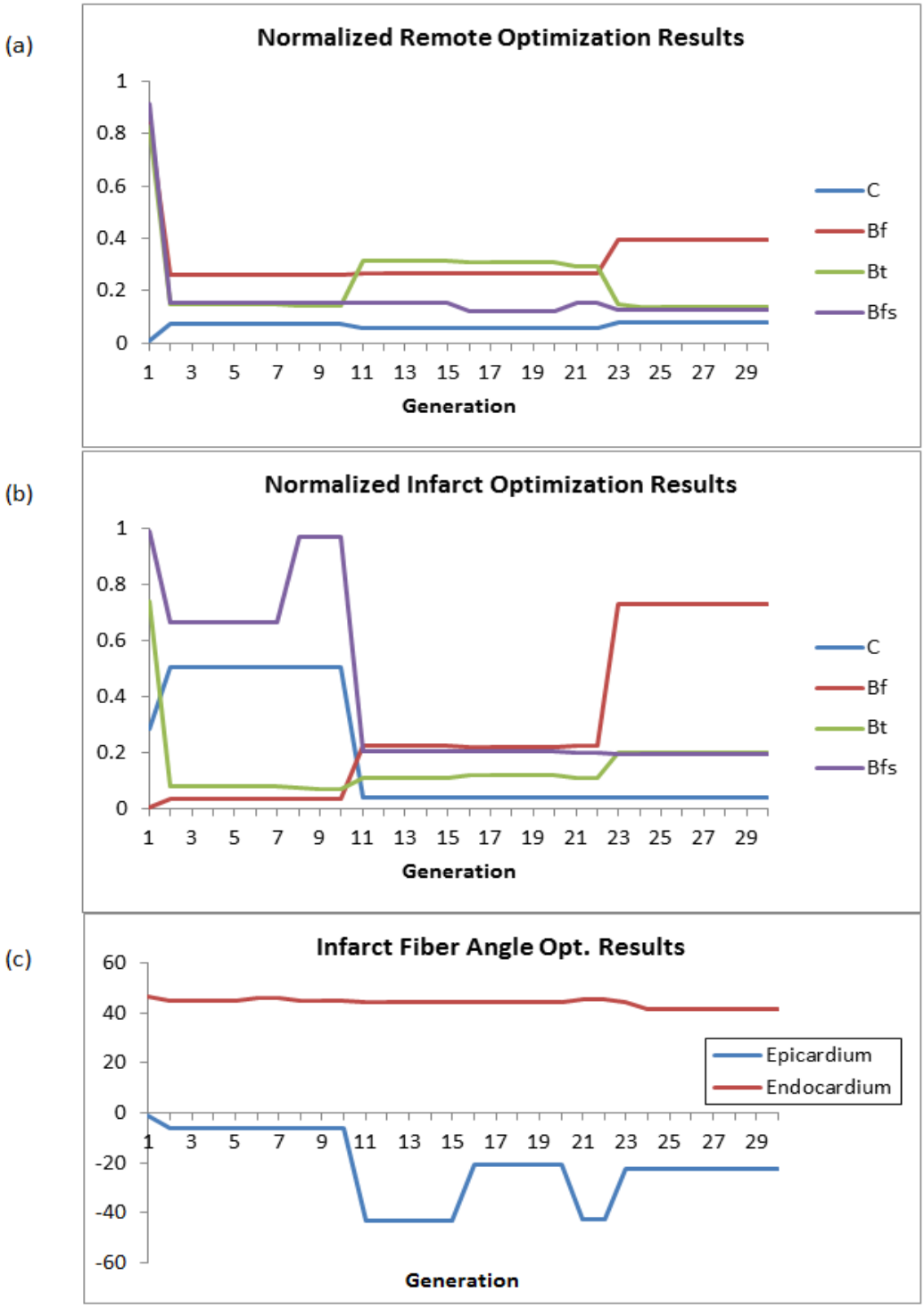

Figure 12: Optimization results by parameter for case 2 at 1 week post-MI. The non-angle values in Table 2 were normalized by their respective ranges allowed by the optimization. Results for the remote region can be seen in (a), whereas the infarct results are in (b) with the angles in (c).

The optimized material parameters for all viable case data are given in Table 2, Table 3, and Table 4 for 1 week, 4weeks, and 8 weeks post-MI respectively. Infarcted regions consistently showed greater values of parameters in the exponential of the constitutive relation used, Equation 3. At 1 week post-MI, each of the cases exhibited a strong degree of anisotropy in the infarct regions. The material parameters showed greater variability at the later time points, but all cases exhibited a softening of the infarct after a rapid increase in stiffness at 1 week post-MI. The infarct angles varied greatly between cases and time points. MSE values varied between 4.28 and 11.62, comparable to values achieved through a similar approach in previous studies.[27,28] In fact, the current approach used 1.5 to 2 times more strain components in the MSE calculation than the previous studies. This implies that the agreement, between the experimentally measured and FE predicted quantities, is better in the current work.

Upon examining the MSE and endo-angle values in Table 3 and Table 4, it can be seen that cases in which the optimized endo-angle laid within 15 degrees of circumferential produced the highest MSE values. These cases were also the only ones which possessed higher values of b_t than b_f in the infarct, implying a greater stiffness in the cross-fiber direction. This is an unintuitive result that cannot be easily explained through natural phenomena, so it makes sense for these particular cases to have the highest MSE results. There appears to be a correlation between the infarct angle at the endocardium and the infarct parameter b_f. The endo-angle also seems to have greater influence on the outcome of the optimization than the epi-angle. Look at the spread of endo-angles in the 1 week post-MI cases of Table 2. They are tightly packed around 42 degrees with a standard deviation of less than 2. Considering this consensus and moving on to the 4 weeks post-MI cases of Table 3, it can be seen that case with the highest MSE is also the odd one of the group. At 4 weeks post-MI, case 3 is the only one with a low endo-angle of 3.9 degrees, whereas the other cases possessed endo-angles ranging between 41 and 49 degrees. The same type of trend can be found in the 8 weeks post-MI results in Table 4.

Results of the simulated equi-biaxial extension tests for each case can be found in Figure 13 through Figure 18. The variability between cases becomes more pronounced at 4 weeks post-MI, but it can still be readily seen that the infarct regions are stiffer than remote regions at each of the time points. The colors for each of the animal cases are used consistently through each of the time points post-MI of the simulated equi-biaxial extension plots, allowing for the time course of a particular animal to be more easily viewed. Only Case 3 had viable data for all 3 time points, but the infarct region appears to soften over the time course after a tremendous increase in stiffness at 1 week post-MI. This observation gains further credibility from the mean plots of equi-biaxial extension simulations in Figure 14, Figure 16, and Figure 18.

The mean plots of equi-biaxial extension simulations show that the infarct and remote regions both soften over the course of healing after an initial spike in stiffness near 1 week post-MI. The anisotropy of the infarct also appears to become less pronounced as time progresses. However upon examining the spread of results for 4 weeks and 8 weeks post-MI in Table 3 and Table 4, this apparent reduction in anisotropy may merely be the result of averaging.

Table 2: 1 week Optimization Results

		Case				
		1	2	3	4	Avg ± Std
Remote	C (kPa)	1.99	4.89	0.917	0.367	2.04 ± 2.02
	b_f	9.93	8.08	12.49	99.31	32.45 ± 44.61
	b_t	2.32	2.78	6.00	38.87	12.49 ± 17.66
	b_{fs}	46.53	7.77	19.81	4.90	19.75 ± 18.98
Infarct	C (kPa)	0.109	1.01	1.20	1.22	0.88 ± 0.53
	b_f	221.8	182.3	112.3	179.8	174.07 ± 45.47
	b_t	55.53	12.02	11.07	31.72	27.58 ± 20.92
	b_{fs}	48.16	11.79	24.62	25.31	27.47 ± 15.13
	epi-angle (deg)	-49.21	-22.31	-0.45	-0.829	-18.20 ± 23.06
	endo-angle (deg)	43.28	41.31	44.66	41.32	42.65 ± 1.64
	MSE	9.30	9.80	11.62	4.28	8.75 ± 3.14

Table 3: 4 week Optimization Results

		Case				
		1	**3**	**5**	**6**	**Avg** ± Std
Remote	**C (kPa)**	3.86	0.81	0.38	5.83	2.72 ± 2.24
	b_f	41.37	56.64	16.67	7.32	30.50 ± 19.56
	b_t	11.28	8.39	13.75	3.87	9.32 ± 3.67
	b_{fs}	26.79	45.43	38.35	2.81	28.35 ± 16.18
Infarct	**C (kPa)**	88.47	2.83	2.38	9.99	25.92 ± 36.24
	b_f	4.03	1.61	24.69	24.49	13.70 ± 10.92
	b_t	3.46	15.50	4.20	3.34	6.63 ± 5.13
	b_{fs}	6.37	12.34	7.55	7.93	8.55 ± 2.26
	epi-angle (deg)	-27.95	-45.00	-0.14	-44.29	-29.34± 18.19
	endo-angle (deg)	48.55	3.90	47.83	41.84	35.53 ± 18.45
	MSE	7.15	10.41	7.52	5.40	7.62 ± 1.80

Table 4: 8 week Optimization Results

		3	**4**	**5**	**6**	**Avg** ± Std
Remote	**C (kPa)**	0.75	0.51	0.32	0.64	0.56 ± 0.16
	b_f	11.51	49.91	15.13	29.99	26.64 ± 15.12
	b_t	6.64	6.53	44.51	12.66	17.59 ± 15.74
	b_{fs}	28.27	34.32	39.97	8.65	27.80 ± 11.80
Infarct	**C (kPa)**	18.19	0.93	7.13	6.22	8.12 ± 6.28
	b_f	1.06	45.52	3.55	25.20	18.83 ± 18.04
	b_t	2.86	11.96	10.59	3.85	7.32 ± 4.00
	b_{fs}	3.76	8.27	51.85	4.07	16.98 ± 20.21
	epi-angle (deg)	-37.90	-0.28	-45.67	-2.17	-21.50 ± 20.47
	endo-angle (deg)	11.34	41.56	13.29	41.50	26.92 ± 14.63
	MSE	8.04	4.41	9.96	6.31	7.18 ± 2.06

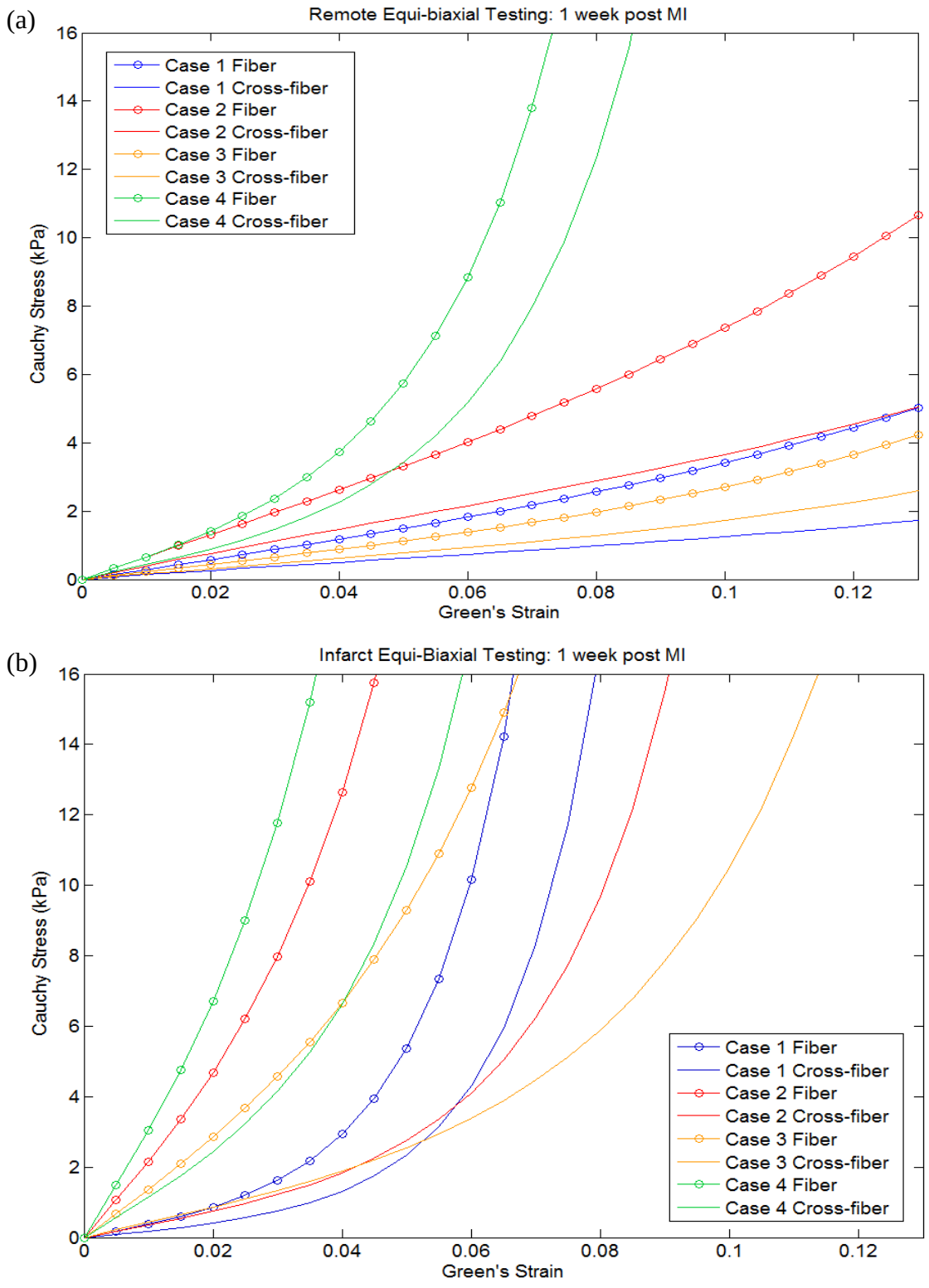

Figure 13: Simulated equi-biaxial extension tests of optimized parameters. The values in Table 2 were input into the constitutive equation, and these plots were then generated using an in-house MATLAB script for biaxial testing. The remote results can be seen in (a) and the results from the infarct region in (b).

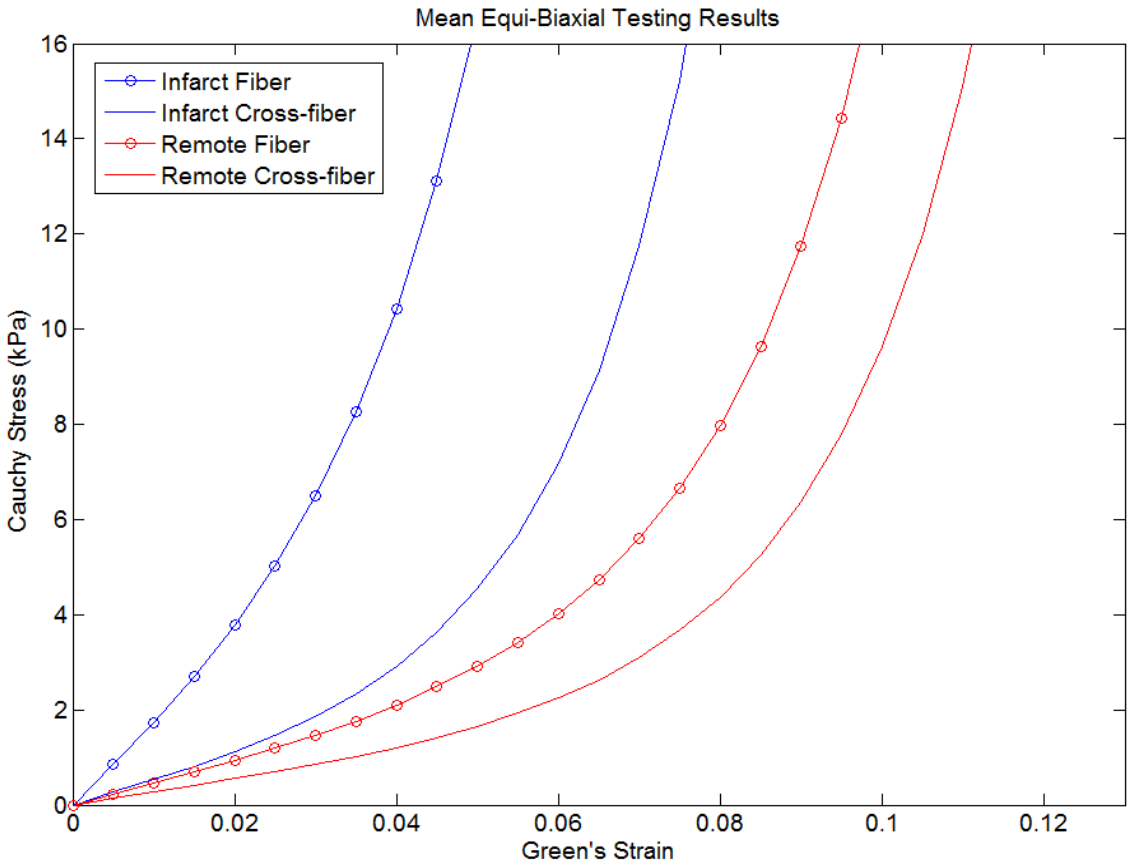

Figure 14: Average stress-strain curves from simulated equi-biaxial extension testing at 1 week post-MI. For each strain point in Figure 13, the corresponding stresses of each case were averaged for the remote and infarcted regions, respectively.

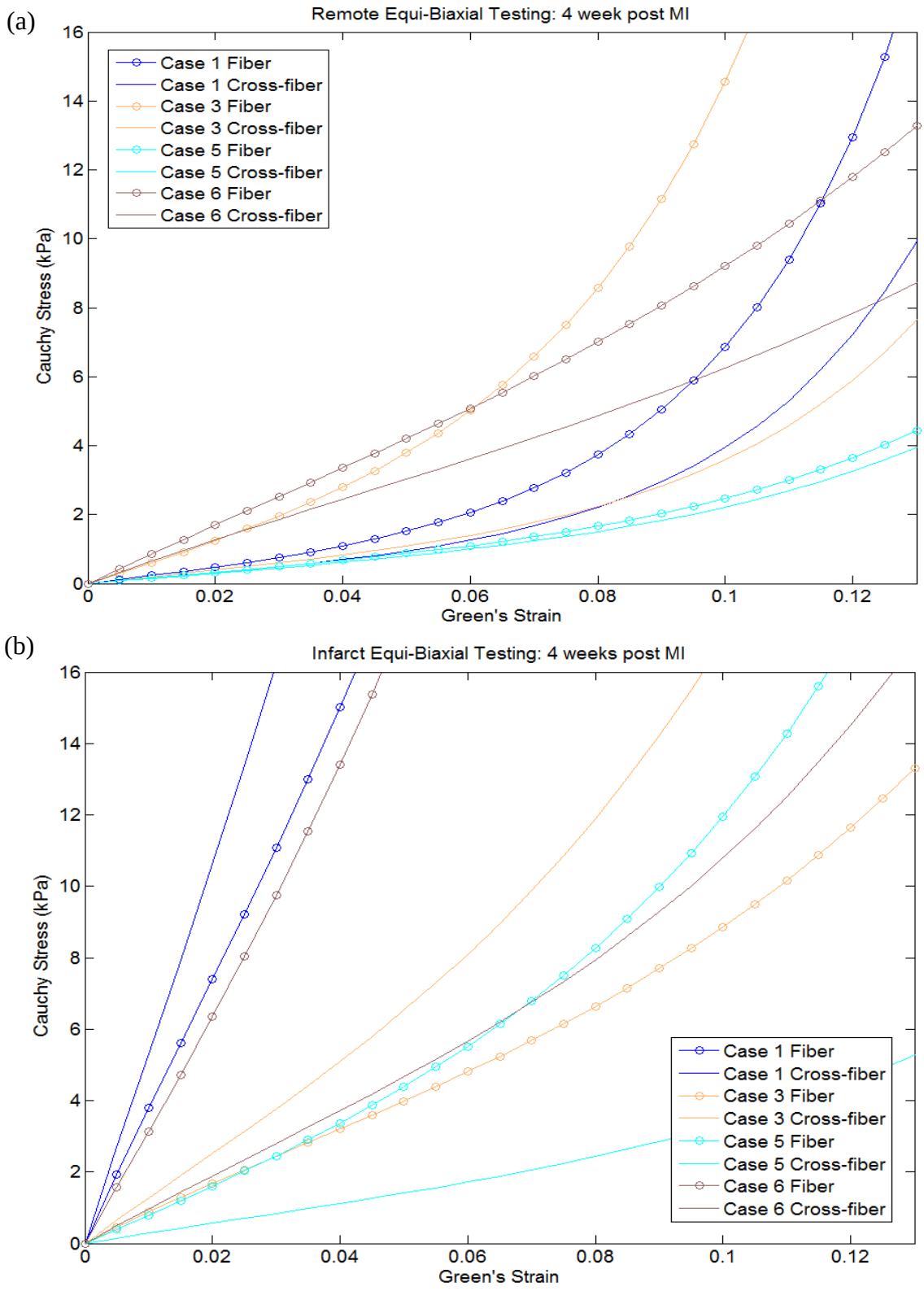

Figure 15: Simulated Equi-biaxial mechanical testing results for (a) remote and (b) infarcted regions at 4 weeks post-MI.

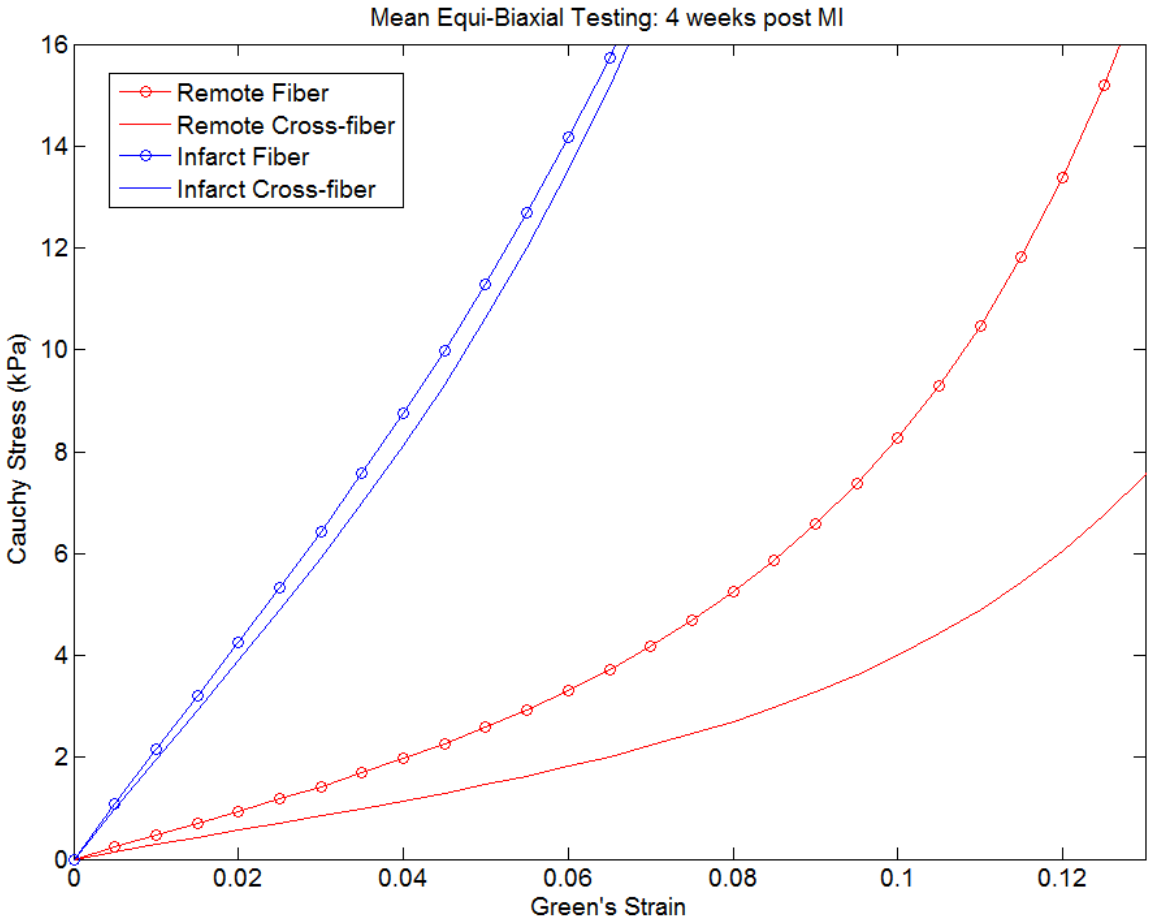

Figure 16: Average stress-strain curves from simulated equi-biaxial extension testing at 4 weeks post-MI. For each strain point in Figure 15, the corresponding stresses of each case were averaged for the remote and infarcted regions, respectively.

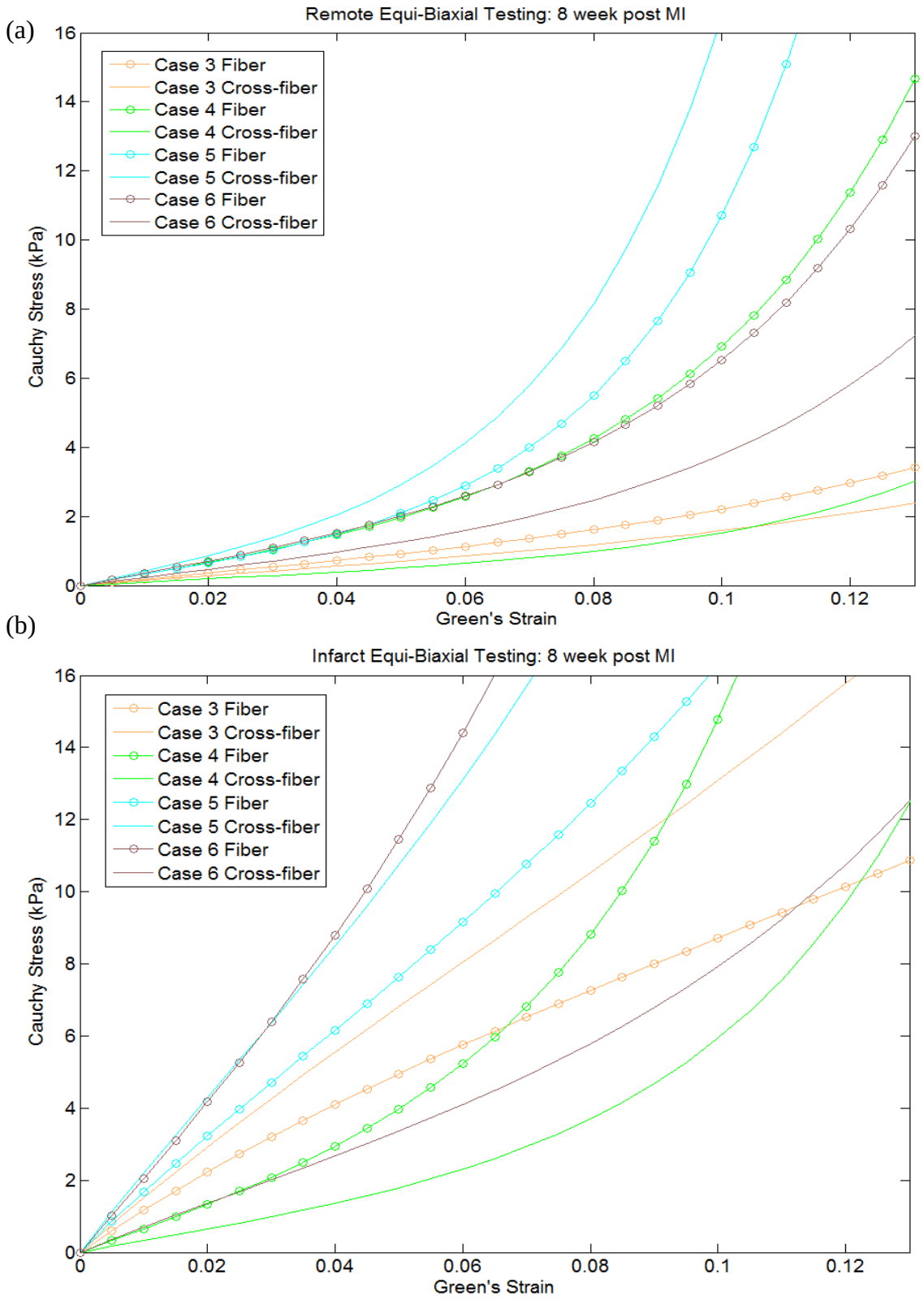

Figure 17: Simulated Equi-biaxial mechanical testing results for (a) remote and (b) infarcted regions at 8 weeks post-MI.

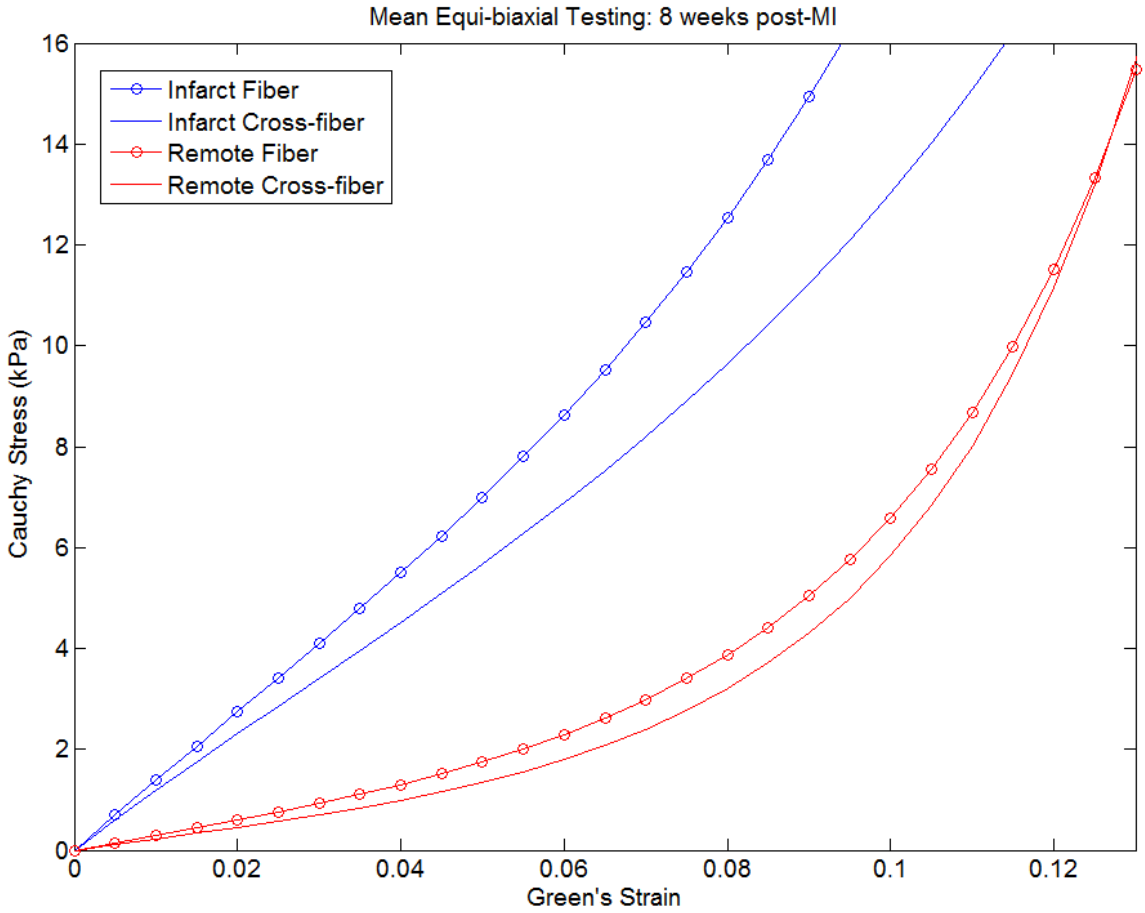

Figure 18: Average stress-strain curves from simulated equi-biaxial extension testing at 8 weeks post-MI. For each strain point in Figure 17, the corresponding stresses of each case were averaged for the remote and infarcted regions, respectively.

4. Discussion

The current study sought to determine in-vivo passive material properties of infarcted and remote myocardium over the course of the remodeling process of a healing MI. The myocardial fiber angle orientation at the endocardial and epicardial surfaces of the infarct were also predicted through an optimization scheme. No other studies were found that incorporated MRI, catheterization, FE modeling, and numerical optimization to estimate both in-vivo passive material properties and infarct fiber orientations. Though few studies have performed experimental biaxial testing on infarcted tissue, Gupta et al. showed that the stiffness of apical aneurysms was much greater than the remote myocardium in sheep 1 week post infarction.[21] In addition, Zhang et al. performed biaxial testing on infarcted tissue from the lateral wall of pig ventricles 2 days post-MI.[33] Those results showed increased extensibility in the cross-fiber direction, which was attributed to fiber disruption and necrosis that occurs within the first few days post-MI.

It can certainly be gathered from the 1 week post-MI results in Table 2 that the infarcted regions initially experience rather significant stiffening and an increase in anisotropy. And this matches well with the timeline of infarct remodeling outlined by Holmes et al.[8] In each of the infarcts at 1 week post-MI, the value of the exponential parameter b_f is significantly greater than the infarct parameters b_t and b_{fs}, implying an increased stiffness in the fiber direction. The changes in stiffness and anisotropy can be much more easily visualized from the simulated equi-biaxial stress-strain curves found in Figure 13 through Figure 18. In Figure 13 it can be seen how the infarcted region has increased in anisotropy at 1 week post-MI, and this is more readily evident in the averaged stress-strain responses of Figure 14.

At 4 weeks post-MI it appears that the infarct may continue to increase in overall stiffness as seen in Figure 14. Case 1 is one of only two for which data was available at 1 week and 4 weeks post-MI. It shows a continued increase in remote and infarct stiffness from 1 week post-MI to 4 weeks post-MI. Shown in Figure 14, the anisotropy of Case 3 actually reverses, and unlike Case 1, the infarct seems to soften from 1 to 4 weeks post-MI.

However, the time course of Case 3 fits quite well with findings of Gupta et al. represented in Figure 3.[21] Notice how in those results, the infarct achieved its maximum

stiffness at 2 weeks post-MI, at which point its anisotropy reverses and the infarct begins to soften. This is very similar to the results of the Case 3 time course, which also exhibits a change in anisotropy and softening, but at 4 weeks post-MI. Since there is no other data on the time course of a healing MI, besides the results of Gupta et al., the exact timing of when an infarct is at its stiffest remains unknown. The data from that study includes times of 2 weeks and 6 weeks post-MI whereas the data of the current study is that of 4 weeks and 8 weeks post-MI.

The infarct collagen fiber architecture predicted in the current study indicates that both the epicardial and endocardial angles become more circumferentially oriented at 1 week post-MI, compared to myofiber angles in the remote region. The endocardial angle shifted from 83 degrees to approximately 43 degrees. As previously mentioned, there is a great consensus between cases for the endocardial infarct angle at 1 week post-MI. This result agrees with findings reported by Holmes et al. (1997) that showed a change in endocardial collagen angles of roughly 32 degrees towards the circumferential direction in pigs 3 weeks post-MI, compared to sham controls. While there is little data in the literature regarding changes in collagen fiber orientation due to MI, the general trend is that fibers become more circumferential over time as the MI remodels.[8]

The coupling of material parameters is inherent to the nature of the constitutive equation used. As can be inferred from Equation 2, the parameter C of the constitutive law popularized by Guccione et al. affects stiffness in all directions. The issue has been previously addressed in studies estimating myocardial material properties using MRI, FE simulation, and optimization. Xi et al. fixed the value of C at 1 kPa, based on the average of previously reported values, and allowed the remaining parameters to optimize independent of C.[37] This was found to produce more consistent results of parameter values between the cases modeled.[37] However in each of the optimizations run in this study, the parameter C for infarct and remote regions was one of the first parameters to plateau to an optimized value. As seen in Figure 11, the parameter C reached its final value as early as the tenth generation with the optimized solution found at the 24th generation.

The results also indicate a coupling between the exponential infarct parameter b_f and the fiber angle at the infarcted endocardium. As seen in Table 2, the endocardial

fibers have an averaged orientation of 42.65 degrees with a standard deviation of only 1.64. Three of the four case results at 4 weeks post-MI have infarcts with endocardial fiber angles ranging between 41 and 49 degrees and a greater stiffness in the fiber direction. These particular cases also have comparably lower MSE values than Case 3, in which there is a greater stiffness in the cross-fiber direction and an endo-angle of only 3.9 degrees. Moving on to the cases at 8 weeks post-MI, the results of Table 4 show that the cases with endocardial infarct angles of around 41, Cases 4 and 6, have significantly lower MSE values than the others, in which the endo-angle was optimized to 11.34 and 13.29 degrees. Again, as with the cases at 4 weeks post-MI, the results that agreed best with experimental data were also those in which there was a greater stiffness in the fiber direction with an endocardial infarct angle of no less than 40 degrees.

This observation appears to fit well with findings by Ursell et al., in which the progression of myocardial damage is heralded by a wavefront of injury moving from endocardium to epicardium.[16] As previously mentioned, in a study by Villareal et al. the magnitude of normal systolic strains was found to increase significantly from epicardium to endocardium in infarcted canine hearts. From mechanobiology, it is known that physical forces acting on cells contribute to changes in structure and function. In regard to a myocardial infarction, the endocardium would be expected to experience structural changes quicker than the epicardium, as the endocardium is exposed to higher strains. This may explain why there appears to be a strong correlation between the endocardial fiber orientation and the infarct parameter b_f, whereas there is not a easily identified trend in epicardial fiber orientation.

There are similarities and differences between the approach in the current study and previous work. MRI and catheterization were used to quantify wall motion and ventricular pressure, respectively, in both the current and previous studies.[27,28,37,38] In every case, finite element models were generated from the MRI-based geometry and loaded with the measured pressure, in order to simulate ventricular deformation. However, in work by Wang et al. (2009) and Xi et al. (2013) wall displacement was used in the optimization, whereas in the current study, and in work by Sun et al. (2009) and Wenk et al. (2011), strain was used to quantify wall deformation in the optimization.[27,28,37,38] Since displacement is the primary value measured by MRI and

strain quantifies only deformation without rigid motion, each approach has distinct advantages.

There are several limitations associated with the approach presented in this work. In the current study, and the study by Xi et al., average myofiber angles were assigned to the myocardium, which does not fully represent the spatially varying fiber architecture.[37] The transmural change in fiber orientation is modeled as linear throughout, and the regional differences, most notably from base to apex, are not included.[32] As seen in Figure 7 and Figure 8 from the study by Mekkaoui et al., the fiber orientations can vary rather non-linearly in the transmural direction of both normal and impaired myocardium.[32] In the future, fiber angles will be based on DTMRI data, similar to the study by Wang et al., in order to incorporate more accurate spatially variation.[38] The reference configuration of the FE model was based on early diastole, where pressure is at a minimum, but the ventricle is still partially loaded. In the future, techniques for determining the unloaded geometry will be incorporated, similar to Krishnamurthy et al.[39] The strain field that was calculated from the 3D SPAMM images contained a small amount noise. This was minimized as much as possible by smoothing the strain at each point of interest with the neighboring values. Despite these limitations, the results of the current work are consistent with those of previous studies.

5. Conclusion

The method used in this paper for the estimation of in-vivo passive material properties and collagen fiber orientation of a myocardial infarction has proven effective. The material properties of the remote region were also able to be determined simultaneously with the optimization. The results agree with observations of previous studies, such as an increase in infarct stiffness at 1 week post-MI. Similarities between the time response of a healing infarction presented in the paper by Gupta et al. and the results of Case 3 are also evident.[21] The results of the infarct fiber orientations were much more varied than the material parameter values, but on average, a trend of the angles shifting to a more circumferential orientation could be seen. For future work, diffusion tensor fiber data for the remote region would likely help the model's accuracy tremendously.

There have been few studies to produce any data on the in-vivo material properties of infarcts, and much less on the properties over the time course of healing. There is also very little data on the fiber orientations of infarcted regions and how they change during the remodeling process. With improvements in these areas, the proposed method for determining in-vivo passive material properties should prove useful in the advancement of knowledge of infarcts and ventricular remodeling as well as the development of intervention therapies.

References

1 Go, A. S. *et al.* Heart Disease and Stroke Statistics--2013 Update: A Report From the American Heart Association. *Circulation* **127**, e6-e245, doi:10.1161/CIR.0b013e31828124ad (2012).

2 Mann, D. L. Mechanisms and Models in Heart Failure : A Combinatorial Approach. *Circulation* **100**, 999-1008, doi:10.1161/01.cir.100.9.999 (1999).

3 Christman, K. L. & Lee, R. J. Biomaterials for the Treatment of Myocardial Infarction. *J Am Coll Cardiol* **48**, 907-913, doi:10.1016/j.jacc.2006.06.005 (2006).

4 Humphrey, J. D. *Cardiovascular solid mechanics : cells, tissues, and organs*. (Springer, 2002).

5 Mullender, M. G. & Huiskes, R. Proposal for the regulatory mechanism of Wolff's law. *J Orthop Res* **13**, 503-512, doi:10.1002/jor.1100130405 (1995).

6 Arem, A. J. & Madden, J. W. Effects of Stress on Healing Wounds .1. Intermittent Noncyclical Tension. *J Surg Res* **20**, 93-102, doi:Doi 10.1016/0022-4804(76)90104-9 (1976).

7 Wickline, S. A., Verdonk, E. D., Wong, A. K., Shepard, R. K. & Miller, J. G. Structural remodeling of human myocardial tissue after infarction. Quantification with ultrasonic backscatter. *Circulation* **85**, 259-268, doi:10.1161/01.cir.85.1.259 (1992).

8 Holmes, J. W., Borg, T. K. & Covell, J. W. Structure and Mechanics of Healing Myocardial Infarcts. *Annual Review of Biomedical Engineering* **7**, 223-253, doi:10.1146/annurev.bioeng.7.060804.100453 (2005).

9 Weisman, H. F., Bush, D. E., Mannisi, J. A., Weisfeldt, M. L. & Healy, B. Cellular mechanisms of myocardial infarct expansion. *Circulation* **78**, 186-201, doi:10.1161/01.cir.78.1.186 (1988).

10 Spotnitz, H. M. Macro design, structure, and mechanics of the left ventricle. *J Thorac Cardiov Sur* **119**, 1053-1077 (2000).

11 Morita, M. *et al.* Modification of infarct material properties limits adverse ventricular remodeling. *The Annals of Thoracic Surgery* **92**, 617-624, doi:10.1016/j.athoracsur.2011.04.051 (2011).

12 Wenk, J. F. *et al.* First finite element model of the left ventricle with mitral valve: insights into ischemic mitral regurgitation. *The Annals of Thoracic Surgery* **89**, 1546-1553, doi:10.1016/j.athoracsur.2010.02.036 (2010).

13 Whittaker, P., Boughner, D. R. & Kloner, R. A. Analysis of healing after myocardial infarction using polarized light microscopy. *Am J Pathol* **134**, 879-893 (1989).

14 Villarreal, F. J., Lew, W. Y., Waldman, L. K. & Covell, J. W. Transmural myocardial deformation in the ischemic canine left ventricle. *Circulation Research* **68**, 368-381, doi:10.1161/01.res.68.2.368 (1991).

15 Xu, C. *et al.* Deformation analysis of 3D tagged cardiac images using an optical flow method. *J Cardiovasc Magn Reson* **12**, 19, doi:10.1186/1532-429X-12-19 (2010).

16 Ursell, P. C., Gardner, P. I., Albala, A., Fenoglio, J. J. & Wit, A. L. Structural and electrophysiological changes in the epicardial border zone of canine myocardial infarcts during infarct healing. *Circulation Research* **56**, 436-451, doi:10.1161/01.res.56.3.436 (1985).
17 Amirhamzeh, M. M., Hsu, D. T., Cabreriza, S. E., Jia, C. X. & Spotnitz, H. M. Myocardial edema: comparison of effects on filling volume and stiffness of the left ventricle in rats and pigs. *The Annals of Thoracic Surgery* **63**, 1293-1297 (1997).
18 Whittaker, P., Kloner, R. A., Boughner, D. R. & Pickering, J. G. Quantitative assessment of myocardial collagen with picrosirius red staining and circularly polarized light. *Basic Res Cardiol* **89**, 397-410 (1994).
19 Rich, L. W., Peter Collagen and Picrosirius Red Staining: A Polarized Light Assessment of Fibrillar Hue and Spatial Distribution. *Brazillian Journal of Morphological Sciences* **22**, 97-104 (2005).
20 Holmes, J. W., Nunez, J. A. & Covell, J. W. Functional implications of myocardial scar structure. *Am J Physiol-Heart C* **272**, H2123-H2130 (1997).
21 Gupta, K. B., Ratcliffe, M. B., Fallert, M. A., Edmunds, L. H. & Bogen, D. K. Changes in Passive Mechanical Stiffness of Myocardial Tissue with Aneurysm Formation. *Circulation* **89**, 2315-2326 (1994).
22 Costa, K. D., Holmes, J. W. & McCulloch, A. D. Modelling cardiac mechanical properties in three dimensions. *Philos T Roy Soc A* **359**, 1233-1250, doi:DOI 10.1098/rsta.2001.0828 (2001).
23 Demer, L. L. & Yin, F. C. Passive biaxial mechanical properties of isolated canine myocardium. *J Physiol* **339**, 615-630 (1983).
24 Humphrey, J. D., Strumpf, R. K. & Yin, F. C. P. Determination of a Constitutive Relation for Passive Myocardium .2. Parameter-Estimation. *J. Biomech. Eng.-Trans. ASME* **112**, 340-346, doi:Doi 10.1115/1.2891194 (1990).
25 Guccione, J. M., McCulloch, A. D. & Waldman, L. K. Passive material properties of intact ventricular myocardium determined from a cylindrical model. *J Biomech Eng* **113**, 42-55 (1991).
26 Augenstein, K. F., Cowan, B. R., LeGrice, I. J. & Young, A. A. Estimation of cardiac hyperelastic material properties from MRI tissue tagging and diffusion tensor imaging. *Lect Notes Comput Sc* **4190**, 628-635 (2006).
27 Sun, K. *et al.* A computationally efficient formal optimization of regional myocardial contractility in a sheep with left ventricular aneurysm. *J Biomech Eng* **131**, 111001, doi:10.1115/1.3148464 (2009).
28 Wenk, J. F. *et al.* Regional Left Ventricular Myocardial Contractility and Stress in a Finite Element Model of Posterobasal Myocardial Infarction. *J. Biomech. Eng.-Trans. ASME* **133**, doi:Artn 044501
Doi 10.1115/1.4003438 (2011).
29 Nair, A. U., Taggart, D. G. & Vetter, F. J. Optimizing cardiac material parameters with a genetic algorithm. *Journal of Biomechanics* **40**, 1646-1650, doi:10.1016/j.jbiomech.2006.07.018 (2007).
30 Witschey, W. R. T. *et al.* Rotating Frame Spin Lattice Relaxation in a Swine Model of Chronic, Left Ventricular Myocardial Infarction. *Magn Reson Med* **64**, 1454-1461, doi:Doi 10.1002/Mrm.22543 (2010).

31 Lee, W. N. *et al.* Mapping Myocardial Fiber Orientation Using Echocardiography-Based Shear Wave Imaging. *Ieee T Med Imaging* **31**, 554-562, doi:Doi 10.1109/Tmi.2011.2172690 (2012).
32 Mekkaoui, C. *et al.* Fiber architecture in remodeled myocardium revealed with a quantitative diffusion CMR tractography framework and histological validation. *J Cardiovasc Magn Reson* **14**, 70, doi:10.1186/1532-429X-14-70 (2012).
33 Zhang, S. *et al.* The Correlation of 3D DT-MRI Fiber Disruption with Structural and Mechanical Degeneration in Porcine Myocardium. *Annals of Biomedical Engineering* **38**, 3084-3095, doi:10.1007/s10439-010-0073-8 (2010).
34 Wu, Y., Zhang, L.-J., Zou, C., Tse, H.-F. & Wu, E. X. Transmural heterogeneity of left ventricular myocardium remodeling in postinfarct porcine model revealed by MR diffusion tensor imaging. *Journal of Magnetic Resonance Imaging* **34**, 43-49, doi:10.1002/jmri.22589 (2011).
35 Rohmer, D., Sitek, A. & Gullberg, G. T. Reconstruction and visualization of fiber and laminar structure in the normal human heart from ex vivo diffusion tensor magnetic resonance imaging (DTMRI) data. *Invest Radiol* **42**, 777-789, doi:10.1097/RLI.0b013e3181238330
00004424-200711000-00008 [pii] (2007).
36 Corporation, L. S. T. LS-OPT User's Manual. **Version 4.2** (February 2012).
37 Xi, J. *et al.* The estimation of patient-specific cardiac diastolic functions from clinical measurements. *Medical Image Analysis* **17**, 133-146, doi:10.1016/j.media.2012.08.001 (2013).
38 Wang, V. Y. *et al.* Modelling passive diastolic mechanics with quantitative MRI of cardiac structure and function. *Medical Image Analysis* **13**, 773-784, doi:10.1016/j.media.2009.07.006 (2009).
39 Krishnamurthy, A. *et al.* Patient-specific models of cardiac biomechanics. *Journal of Computational Physics* **244**, 4-21, doi:10.1016/j.jcp.2012.09.015 (2013).

Vita

Dimitri Mojsejenko was born in Owensboro, Kentucky. He entered the University of Kentucky in Lexington, Kentucky in 2007 after graduating from Daviess County High School. He received the degree of Bachelor of Science in Mechanical Engineering at the University of Kentucky in December 2011. He then entered graduate school in the spring of 2012 at the University of Kentucky and began working as a research assistant under Dr. Jonathan F. Wenk in the Mechanical Engineering department. He co-authored a paper published in The Annals of Thoracic Surgery titled “Biventricular Finite Element Modeling of the Acorn CorCap Cardiac Support Device on a Failing Heart” in 2013. In 2014, he was also co-author of the paper “Estimating Passive Mechanical Properties in a Myocardial Infarction using MRI and Finite Element Simulations,” submitted to Biomechanics and Modeling in Mechanobiology.